Computational and Structural Biotechnology Journal 23 (2024) 2995–3018

Contents lists available at ScienceDirect

Computational and Structural Biotechnology Journal

journal homepage: www.elsevier.com/locate/csbj

Simulation- and AI-directed optimization of 4,6-substituted 1,3,5-triazin-2(1*H*)-ones as inhibitors of human DNA topoisomerase IIα

Barbara Herlah [a,b], Tjaša Goričan [a], Nika Strašek Benedik [b], Simona Golič Grdadolnik [a], Izidor Sosič [b], Andrej Perdih [a,b,*]

[a] National Institute of Chemistry, Hajdrihova 19, SI 1000 Ljubljana, Slovenia
[b] University of Ljubljana, Faculty of Pharmacy, Aškerčeva 7, SI 1000 Ljubljana, Slovenia

ARTICLE INFO

Keywords:
Molecular design
Molecular simulations
Deep learning
Human DNA topoisomerase IIα
Catalytic inhibitors
Anticancer agents

ABSTRACT

The 4,6-substituted-1,3,5-triazin-2(1*H*)-ones are promising inhibitors of human DNA topoisomerase IIα. To further develop this chemical class targeting the enzymeś ATP binding site, the triazin-2(1*H*)-one substitution position 6 was optimized. Inspired by binding of preclinical substituted 9*H*-purine derivative, bicyclic substituents were incorporated at position 6 and the utility of this modification was validated by a combination of molecular simulations, dynamic pharmacophores, and free energy calculations. Considering also predictions of Deepfrag, a software developed for structure-based lead optimization based on deep learning, compounds with both bicyclic and monocyclic substitutions were synthesized and investigated for their inhibitory activity. The SAR data showed that the bicyclic substituted compounds exhibited good inhibition of topo IIα, comparable to their mono-substituted counterparts. Further evaluation on a panel of human protein kinases showed selectivity for the inhibition of topo IIα. Mechanistic studies indicated that the compounds acted predominantly as catalytic inhibitors, with some exhibiting topo IIα poison effects at higher concentrations. Integration of STD NMR experiments and molecular simulations, provided insights into the binding model and highlighted the importance of the Asn120 interaction and hydrophobic interactions with substituents at positions 4 and 6. In addition, NCI-60 screening demonstrated cytotoxicity of the compounds with bicyclic substituents and identified sensitive human cancer cell lines, underlining the translational relevance of our findings for further preclinical development of this class of compounds. The study highlights the synergy between simulation and AI-based approaches in efficiently guiding molecular design for drug optimization, which has implications for further preclinical development of this class of compounds.

1. Introduction

Alongside cardiovascular diseases, cancer is one of the most common causes of death worldwide. Of the approximately 60 million deaths reported each year, around 10 million are directly attributable to cancer [1,2]. Cancer is the result of a multistep transformation of normal cells into tumor cells through a series of acquired functional abilities that allow cancer cells to survive, proliferate and spread, also known as the "*Hallmarks of Cancer*" [3,4,8]. The development of cancer can be caused by external influences such as ionizing radiation, various chemicals and biological carcinogens. In addition, the incidence of cancer increases dramatically with age due to a less efficient cell repair machinery [4].

One of the hallmarks of cancer cells is rapid and uncontrolled cell division. This process is highly dependent on the proper function of a large family of enzymes, the DNA topoisomerases, which catalyze topological changes of the DNA molecule [5,6]. In addition, these molecular motors are also involved in the transcription and chromosome division and thus represent a crucial molecular motor for cell survival [7,8]. A well-known subdivision into type I and type II topoisomerases is based on whether they can form transient single-strand or double-strand breaks in the DNA molecule [7,9]. In most cases, topoisomerases enable the simplification of the DNA topology [7]. Like its other isoform, topo IIβ, human DNA topoisomerase IIα (topo IIα) (Fig. 1 A) belongs to the type II class. Both isoforms show high sequence similarity, however the topo IIβ isoform is expressed in quiescent and proliferating cells, whereas topo IIα is predominantly expressed in the latter, making it an attractive drug target that is commonly used in chemotherapy [10–12].

The topo II inhibitors used in clinical practice mainly belong to the

* Corresponding author at: National Institute of Chemistry, Hajdrihova 19, SI-1001 Ljubljana, Slovenia.
E-mail address: andrej.perdih@ki.si (A. Perdih).

https://doi.org/10.1016/j.csbj.2024.06.037
Received 3 May 2024; Received in revised form 29 June 2024; Accepted 30 June 2024
Available online 6 July 2024

group of anthracyclines such as daunorubicin and doxorubicin and the epipodophyllotoxins such as etoposide and teniposide. These compounds mostly act as stabilizers of the short-lived covalent complex between the enzyme and the cleaved DNA, leading to permanent breaks in the DNA and the induction of apoptosis [13]. This approach is frequently used in clinical practice with chemotherapeutic agents to treat various types of cancer such as colorectal cancer, small cell lung cancer, ovarian cancer and hematologic cancer [13,14]. However, their clinical use is often associated with secondary malignancies and cardiotoxicity due to DNA damage and the accumulation of DNA double-strand breaks (DSBs) [15,16]. To overcome this drawback, a diverse group of catalytic inhibitors are currently being developed that utilize different inhibitory mechanisms compared to topo II poisons [9,13]. Within this group, compounds that inhibit ATP binding at the ATPase domain of topo IIα are one of the most attractive and widely explored options. Currently, no compounds that act via this mechanism are used in chemotherapy [9].

One of the projects to develop an ATP-competitive catalytic inhibitor that led to a preclinical drug candidate started with the 9*H*-purine fragment, which was identified in the first screening and further optimized [17]. The addition of quinoline and isopropyl substitutions at the corresponding positions of the purine core significantly improved the overall inhibitory properties. In the final step, a morpholino-ethoxy moiety was added to the resulting lead compound to improve solubility. The result was the preclinical candidate **QAP 1**, for which enzymatic and cellular assays showed very favorable properties for cancer therapy (Fig. 1B) [17].

The 9*H*-purine-based catalytic inhibitors inspired one of our research directions for the development of catalytic inhibitors. The main goal of the molecular design was to find substitutes for the bicyclic core, which in many ways resembles the architecture of human protein kinase inhibitors that also target their corresponding ATP binding sites. Using a pharmacophore-based molecular design, we first discovered 4,6-disubstituted-1,3,5-tiazines that possessed topo IIα inhibitory and cytotoxic properties [19]. Subsequent optimization of the triazine scaffold led to closely related 4,6-substituted-1,3,5-triazin-2(1*H*)-ones with a different monocyclic core designed to mimic the functionality of the adenine moiety. For this class, we confirmed that it binds to the isolated ATPase domain of topo IIα and acts as a catalytic inhibitor [20]. Further structure-guided optimization of the 1,3,5-triazin-2(1*H*)-one substitution position 4 (R^2) resulted in active compounds with some cytotoxicity against the human cancer cell lines HepG2 and MCF-7, which did not induce DNA double-strand breaks (DSB) and thus acted via a mechanism distinct from topo II poisons at the cellular level (Fig. 1 C) [21].

Here the molecular design of the 4,6-substituted 1,3,5-triazin-2(1*H*)-ones was further addressed by focusing on the R^1 substitution pattern located at position 6 of the monocyclic scaffold (Fig. 1 C). In one direction, we took inspiration from the catalytic inhibitor of topo IIα **QAP 1** and incorporated bicyclic substituents at position 6 of the triazin-2(1*H*)-one ring, while retaining the most favorable substituents at position 4 from our previous study [21]. Molecular simulations of the modeled substituted triazin-2(1*H*)-ones were used to evaluate their suitability for binding. To additionally explore the possible R^2 substitutions, we also utilized DeepFrag [22,23], a software based on deep convolutional neural networks specifically designed for structure-based lead optimization. The results of simulation and AI-based optimization guided the selection of new 4,6-substituted-1,3,5-triazin-2(1*H*)-ones for synthesis. The analogs obtained were then investigated in various biochemical and biophysical assays to evaluate their mechanism of inhibition. Binding to the ATPase domain was studied by STD NMR to better support the computationally determined binding models and to reveal the details of molecular recognition. Finally, the cytotoxic profile of the class was investigated in a panel of 60 human cancer cell lines (NCI-60) to fully characterize the current potential of this class of catalytic inhibitors for the development of chemotherapeutic regimens.

2. Results and discussion

2.1. Molecular simulations and deep learning for the optimization of 4,6-substituted-1,3,5-triazin-2(1H)-ones

In the search for ideas to further optimize the 4,6-substituted-1,3,5-

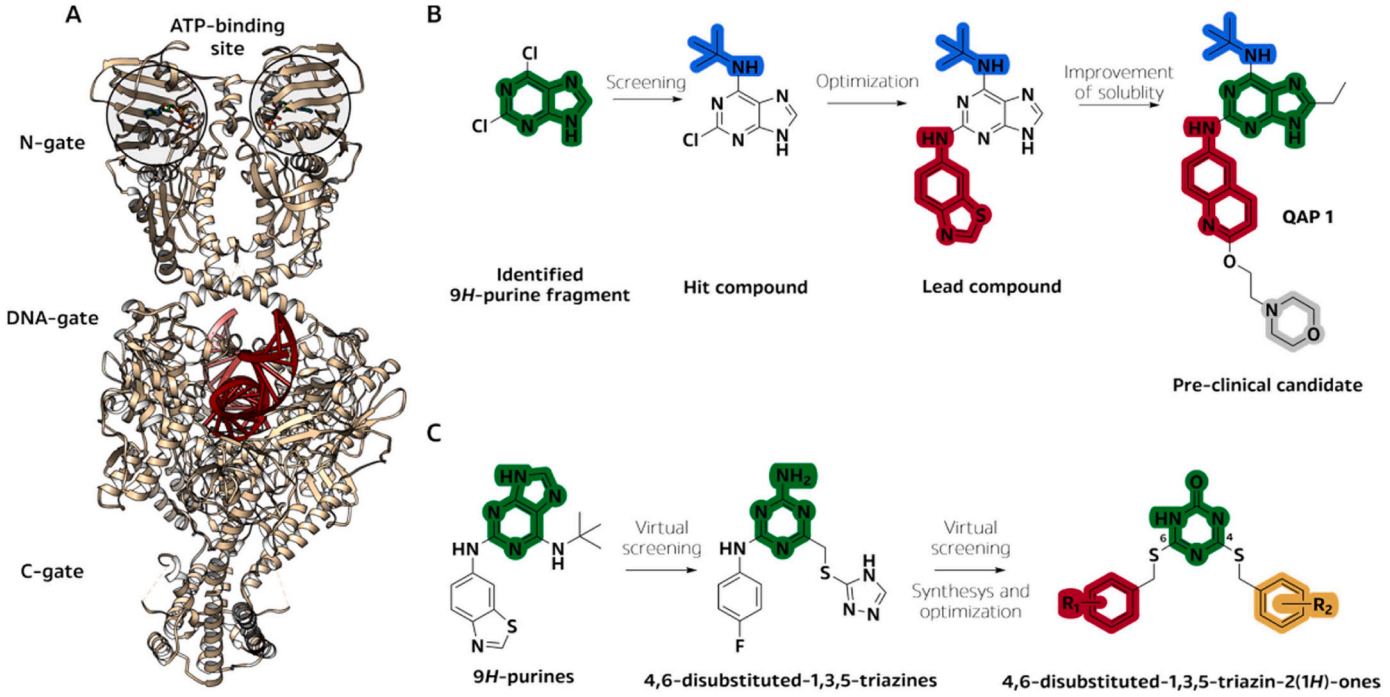

Fig. 1. (**A**) Cryo-EM structure of the fully catalytic human DNA topoisomerase IIα (PDB: 6ZY8) with labelled gates and the ATP binding site [18]. (**B**) Development of bicyclic catalytic inhibitors of human topoisomerase IIα containing a 9*H*-purine scaffold targeting the ATP binding site, leading to the preclinical candidate **QAP 1**. (**C**) Development of the 4,6-substituted-1,3,5-triazin-2(1*H*)-ones as monocyclic catalytic inhibitors inspired by 9*H*-purines.

triazin-2(1*H*)-ones, we again resorted to the 9*H*-purine series and docked the preclinical **QAP 1** in the ATP binding site of topo IIα [24] and compared its conformation with that of the 4,6-substituted-1,3,5-triazin-2(1*H*)-one with a 3-chlorophenyl substituent at R^1 (position 6) and 3-trifluoromethyl-5-fluorobenzyl at R^2 (position 4), a derivative resulting from the optimization of R^2 (Fig. 2A) [21]. Our **QAP 1** docking binding model was consistent with the binding model reported for the 9*H*-purine compounds without the 2-morpholinoethoxy moiety [25]. The experimental data showed competitive ATP inhibition of **QAP 1** and provided further support for the generated poses. In the case of the triazinone class, microscale thermophoresis (MST) experiments provided evidence that the compounds bind to the isolated topo IIα ATPase domain [20].

The triazin-2(1*H*)-one and 9*H*-purine scaffolds overlapped, and both interact with the Asn120, mimicking the interaction with the adenine of ATP. The substituted quinolin-6-yl moiety bound to the 9*H*-purine core of **QAP 1** is aligned with the 3-chlorophenyl substituent at the R^1 position of the triazinone. Both form hydrophobic interactions with Ile125 and Pro126, which are located in a region bellow of the adenine portion of the ATP binding site. The 2-morpholinoethoxy moiety of **QAP 1**, which was incorporated to improve solubility, was located in the bulk, as expected. The optimized R^2 substituent interacted with Ser148, Ser149, Asn150 of the ribose sub-pocket, and Asn91, as well as residues Arg162-Lys168, which interact with the ATP phosphate moiety [24]. In addition, the isopropyl substituent of **QAP 1** interacted with a vacant hydrophobic pocket above the ATP adenine moiety, which is currently

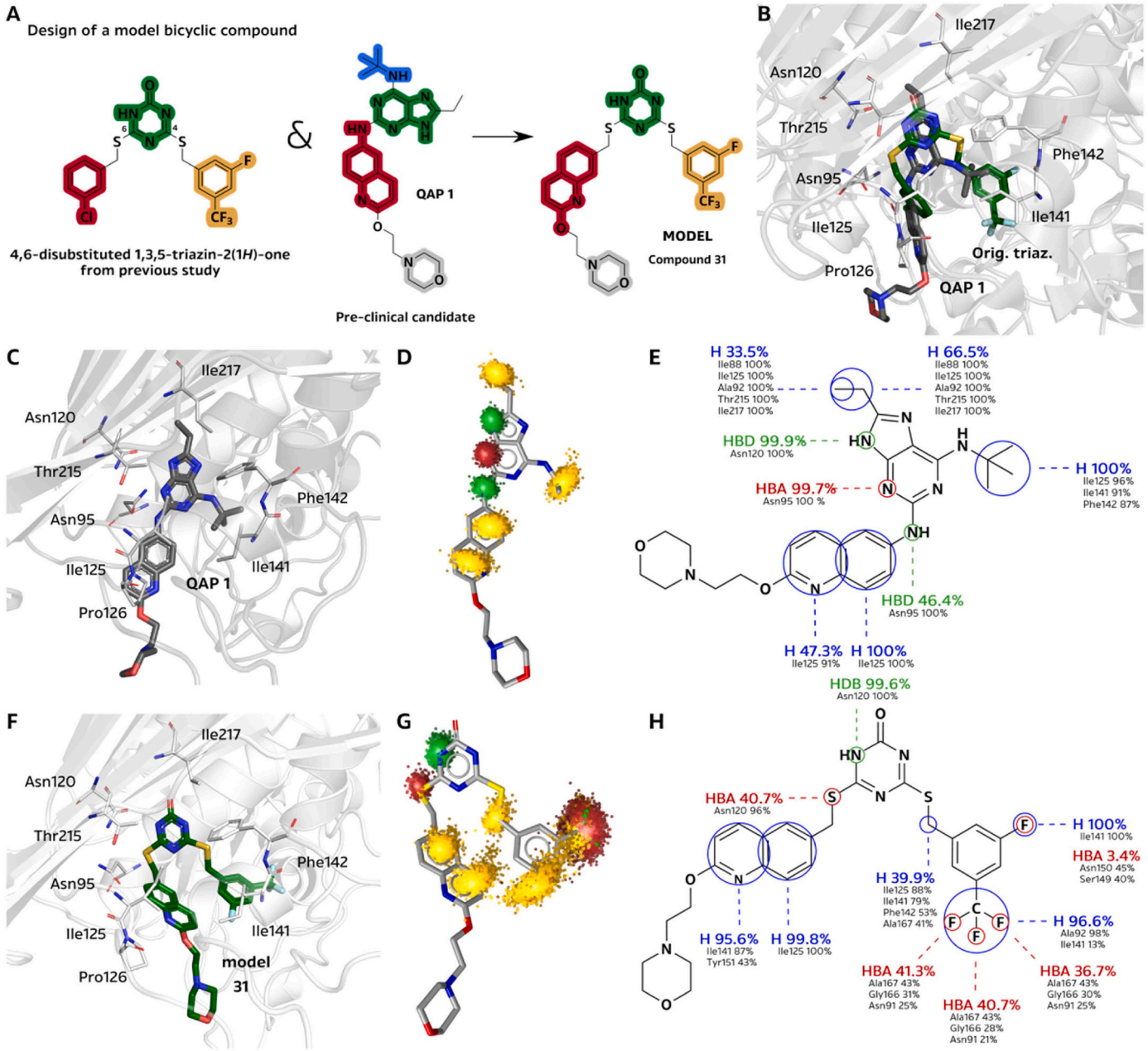

Fig. 2. Simulation-based optimization of 4,6-substituted-1,3,5-triazin-2(1*H*)-ones. (**A**) Outline of the design of the novel **model** (**31**) compound incorporating the structural data of the 4,6-substituted 1,3,5-triazin-2(1*H*)-one from our previous study and 9*H*-purine-based catalytic topo IIα inhibitor **QAP 1**. (**B**) Docking conformations of **QAP 1** (grey) and 4,6-substituted 1,3,5-triazin-2(1*H*)-one from our previous study (green) compounds in the ATP binding site. (**C**) MD snapshot of the **QAP 1** compound in the ATP binding site. (**D**) 3D dynophore model and (**E**) 2D scheme of the dynophore model. (**F**) MD snapshot of the **model** (**31**) compound in the ATP binding site. (**G**) 3D dynophore model and (**H**) 2D scheme of the dynophore model. Hydrophobic features are yellow, hydrogen bond donors are green, and hydrogen bond acceptors are red.

not targeted by our compounds. The docking comparison clearly showed that similar bicyclic substituents can also be incorporated at position 6 of the triazinones (Fig. 2). Therefore, we decided to keep the already optimized 3-trifluoromethyl-5-fluorobenzyl moiety at position 4, and introduce a 2-morpholinoetoxy-substituted quinolin-6-yl moiety at position 6 of the 1,3,5-triazinone which resulted in a **model** compound (**31**) (Fig. 2A).

Unfortunately, no crystal structures with bound 4,6-substituted-1,3,5-triazin-2(1*H*)-one or any inhibitor at all other than the non-hydrolyzable ATP analogue ANP-PNP and ADP at the ATP binding site of topo IIα are available so far. To explore the dynamic component of molecular recognition between the ligands and the ATP binding site of topo IIα and to overcome the limitations of conventional static methods of molecular design such as molecular docking and pharmacophore modelling [26–28], molecular dynamics (MD) simulations with a duration of 0.5 μs were performed for docking poses of compounds **QAP 1** and **model** (**31**) (Fig. 2B). The root-mean square deviation (RMSD) with average values of 2.4 ± 0.7 Å and 2.2 ± 0.3 Å for the **QAP 1** and **model** compounds, respectively, indicates similar pose stability.

To analyze the dynamic and energetic components of molecular recognition of both ligands, dynamic pharmacophore models (i.e., dynophores) and Molecular Mechanics/Generalized Born Surface Area (MM/GBSA) free energy calculations were employed (Table 1). Dynophores are an integration of the structure-based pharmacophore models derived for the bound ligand in each frame of the trajectory. They represent an efficient geometry-based technique to model the dynamics of ligand-receptor molecular recognition. However, as this approach does not provide information about the energetics of the binding process, MM/GBSA calculations can nicely supplement these results using the same MD trajectory. The MM/GBSA method estimates the free energy of binding of ligands to biomolecules by combining molecular mechanics (MM) energies with solvation effects modeled by the Generalized Born (GB) implicit solvent model and Surface Area (SA) contributions to account for non-polar solvation effects, along with entropy contributions typically derived from normal mode analysis or quasi-harmonic approximations. Rooted in a thermodynamic cycle, MM/GBSA also enables energy decomposition that can yield insights into the contributions of individual residues to the overall binding affinity. As methods are based on a different premise they can yield complementary results (e.g. identifying a residue with an important contribution overlooked by pharmacophores) thereby enhancing the understanding of the receptor-ligand binding process.

In the **QAP 1** molecule, 9*H*-purine scafold can form stable hydrogen bonds with both Asn120 and Asn95, which are present throughout the trajectory, with the Asn120 interaction being the most favorable from an energetic point of view. The dynophore model showed three clusters of hydrophobic interactions between the ethyl, isopropyl, and quinolin-6-yl elements bound to the core scaffold and residues such as Ile88, Asn91, Ile125, Ile141, and Phe142. These residues were also energetically favorable for the interaction, especially Ile125 and Ile141. The MM/GBSA calculation also revealed a favorable interaction with Pro126, the residue in the hydrophobic sub-pocket below the adenine moiety, and Tyr151. The 2-morpholinoethoxy moiety remained outside the binding site and showed no interactions with the ATP binding site, which is consistent with its function to improve physicochemical properties, particularly solubility (Fig. 2C-E and Table 1).

Table 1
Per-residue decomposition of the free energy of binding of **QAP 1** and **model** (**31**) compounds with listed residues that compounds interact most favorably.

Residue	Energy contribution [kcal/mol] QAP 1	Energy contribution [kcal/mol] Model compound
Ile88	-1.3 ± 0.3	-1.3 ± 0.5
Asn91	-1.6 ± 0.6	-1.3 ± 0.8
Ala92	-0.9 ± 0.3	-1.2 ± 0.3
Asn95	-1.9 ± 0.9	-0.9 ± 0.5
Asn120	-4.5 ± 0.5	-3.0 ± 0.5
Ile125	-3.8 ± 0.4	-2.1 ± 0.6
Pro126	-2.3 ± 0.5	-1.1 ± 0.5
Ile141	-0.5 ± 0.3	-2.6 ± 0.7
Phe142	-1.6 ± 0.5	-1.2 ± 0.2
Tyr151	-1.1 ± 1.0	-1.1 ± 1.1
Thr215	-1.5 ± 0.4	-1.2 ± 0.3
Ile217	-1.2 ± 0.3	-0.9 ± 0.2

As in the **model** (**31**) compound, the amide nitrogen on the triazinone ring and a connecting sulfur atom provide stable hydrogen bonds with Asn120. However, according to MM/GBSA, their contribution is 1.5 kcal/mol lower than in the case of **QAP 1**. In addition, the 3-trifluoromethyl moiety at the phenyl at position 4, forms multiple hydrogen bonds as its three fluorine atoms oscillate between residues Asn91, Ser149, Asn150, Gly166, and Ala167. Hydrophobic interactions between the quinolin-6-yl (at position 6 of the 1,3,5-triazinone) and 3-trifluoromethyl-5-fluorobenzyl substituents and the residues Ala92, Ile125, Ile141, Phe142, Tyr151, and Ala167 were detected with the dynophore. Interactions with Ile125 and Ile141 were particularly favorable from the energy standpoint. MM/GBSA again determined a favorable energetic contribution of Pro126 to the binding of the R^1 bicyclic pattern. Residues, such as Ile88, Thr215, and Ile217, which interact predominately with the triazinone core, also exhibited a noticeable contribution. In contrast to the dynophore, no significant binding contribution of residues Ser149 and Asn150 was observed in MM/GBSA calculations (Fig. 2F-H and Table 1).

Overall, both dynophore and MM/GBSA calculations indicate that the introduction of bicyclic substituents at R^1 (position 6) leads to stable and productive binding in the ATP binding site of the topo IIα. The total energy of **QAP 1** was generally more favorable compared to the **model** (**31**) compound, suggesting that the designed triazinones would still not lead to higher IC_{50} values than those determined for 9*H*-purines. However, the triazinones synthesized so far contain substituted phenyls that are poorly soluble, which compromises their utility for further development. Therefore, the introduction of substituents which could improve this aspect is central. Considering the results of the simulation-based molecular design, we decided to synthesize the **model** (**31**) compound together with compounds **24**–**33** to investigate the effect of introducing bicyclic-type R^1 substituents more comprehensively. The R^2 substituents that were incorporated into these target molecules were 3-trifluoromethyl-5-fluorobenzyl, 4-isopropylbenzyl, and 4-trifluoromethyl, all of which showed favorable properties for this substitution position in our optimization study [21].

Artificial intelligence (AI) tools, especially deep learning, are currently gaining popularity in all branches of science, with medicinal chemistry and drug development being no exception [29]. Among the tools that can enable effective lead optimization is the recently developed DeepFrag software, which was developed specifically for this purpose and is based on a deep learning architecture. It defines a specific atom on a ligand site that serves as a 'growth point of interest' and then uses a deep learning architecture to append its possible fragments, which are ranked based on the most suitable interactions [22,23,30].

The use of Deepfrag was also initiated from the docking pose of 4,6-substituted-1,3,5-triazin-2(1*H*)-one with 3-chlorobenzyl substituent at position 6 and optimized 3-trifluoromethyl-5-fluorobenzyl at position 4 (Fig. 3A, S1). The defined 'growth point of interest' was the carbon atom at position 6 next to the linker sulfur atom (Fig. 3A, S1). In the list of the most favorable fragments provided by Deepfrag were substituted phenyls, some of which were already integrated into our molecules (Table S1). In this respect, Deepfrag already provided leverage for such substituents. As mentioned earlier, the compounds synthesized with such R^1 substituents had suboptimal physical chemical properties and their SAR was already quite substantially explored. For this reason, we primarily focused on the introduction of bicyclic substituents at R^1. However, as we also wanted to make a comparison in this study, a new derivative (compound **34**) was synthesized with a benzyl-based

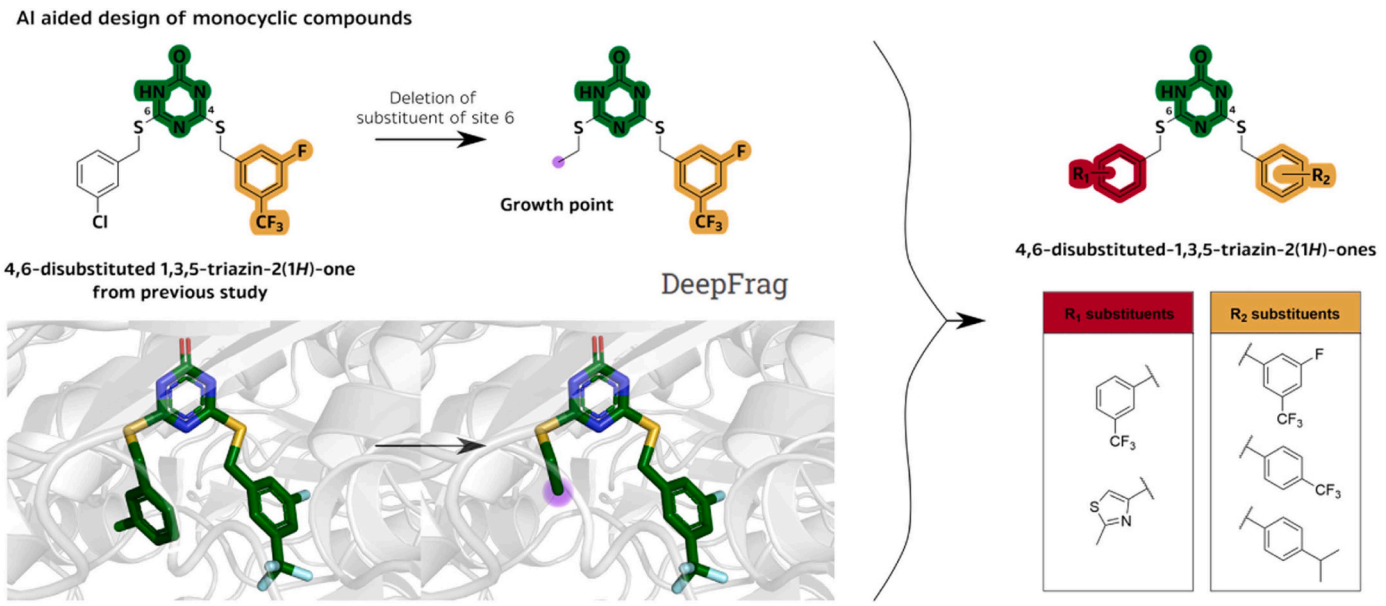

Fig. 3. Optimization of 4,6-substituted-1,3,5-triazin-2(1*H*)-ones using Deepfrag based on AI. Definition of the 'growth point of interest' from the docking pose of the starting triazinone compound with monocyclic R^2 substituent in the ATP binding site and selection of compounds with monocyclic R^2 substituent for synthesis considering the Deepfrag results.

substituent at position 6. We chose to incorporate the CF_3 group at position 3 of the phenyl ring, a moiety that is favorable in terms of metabolism, and in Deepfrag's predictions. Since no heterocyclic monocyclic substituents had been identified as favorable by Deepfrag, we decided to test this by inserting a five-membered thiazole heterocycle at position 6, thereby providing a reasonable phenyl isostere with improved solubility. All three of the aforementioned R^2 substituents were utilized at the position 4, resulting in the synthesis of target compounds **34**–**37**. The topo IIα inhibition properties of these three compounds would ultimately serve to some crude extent validate the Deepfrag predictions prospectively, as lower inhibition activity is expected.

2.2. Synthesis of targeted compounds

The synthetic route to the proposed 4,6-disubstituted-1,3,5-triazin-2(1*H*)-ones was already described and thoroughly elaborated [31]. Nevertheless, to further explore the chemical space at positions 6 of the core triazinone, a greater diversity of S-substituted thiourea analogs was required. To achieve this, we either used commercially available halogenated heterocycles (see Scheme 2) or synthesized them (compounds **1**–**3**, **7**) from methylated precursors by employing different bromination procedures (Scheme 1).

The subsequent reaction of halogenated derivatives with thiourea in MeCN at 80 °C afforded readily S-substituted thiourea analogs **8**–**15** in good yields (Scheme 2), with the exception of 3-(bromomethyl)− 5-chlorobenzo[*b*]thiophene. In this case, two distinct products **13a** and **13b** were observed in the proton NMR after completion of the reaction, and the molar ratio of **13a**/**13b** was 0.26. We did not separate the two products at this stage and proceeded to the next reaction steps using a mixture of **13a** and **13b**.

The 6-substituted 4-mercapto-1,3,5-triazin-2(1*H*)-ones **16**–**23** were then synthesized by cyclization of thiourea derivatives **8**–**15** with ethoxycarbonyl isothiocyanate in the presence of 2 M NaOH in toluene at room temperature (Scheme 3).

It is noteworthy that for the preparation of compound **18** different conditions were used to obtain the triazinone ring, i.e. KO*t*Bu as base and THF as solvent. In the final reaction step, the substituent at position 4 was introduced by alkylation with various benzyl bromides in a basic EtOH solution at room temperature (Scheme 4), leading to the final compounds **24**–**37** (Table 1). The morpholinoethoxy side chain (in compound **31**) was introduced by a nucleophilic aromatic substitution at the 2-chloroquinoline moiety of **30**.

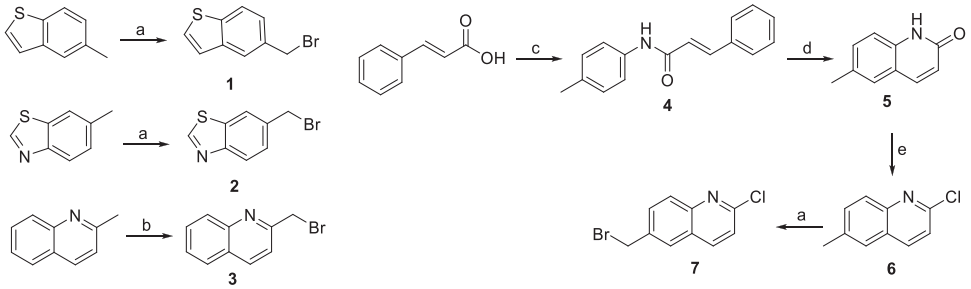

Scheme 1. Preparation of brominated building blocks **1**, **2**, **3**, and **7**. Reagents and conditions: (a) NBS, DBPO, CCl_4, 80 °C, 2 h (for **1**) or CCl_4, rt, 4 h (for **2**) or benzene, 80 °C, 1 h (for **7**); (b) CuBr, TBHP, MeCN, 70 °C, overnight; (c) step 1: $SOCl_2$, toluene, 80 °C, 2 h; step 2: *p*-toluidine, $NaHCO_3$, DMAP, THF, rt, 24 h; (d) $AlCl_3$, 100 °C, 1 h; (e) $POCl_3$, 110 °C, 1 h.

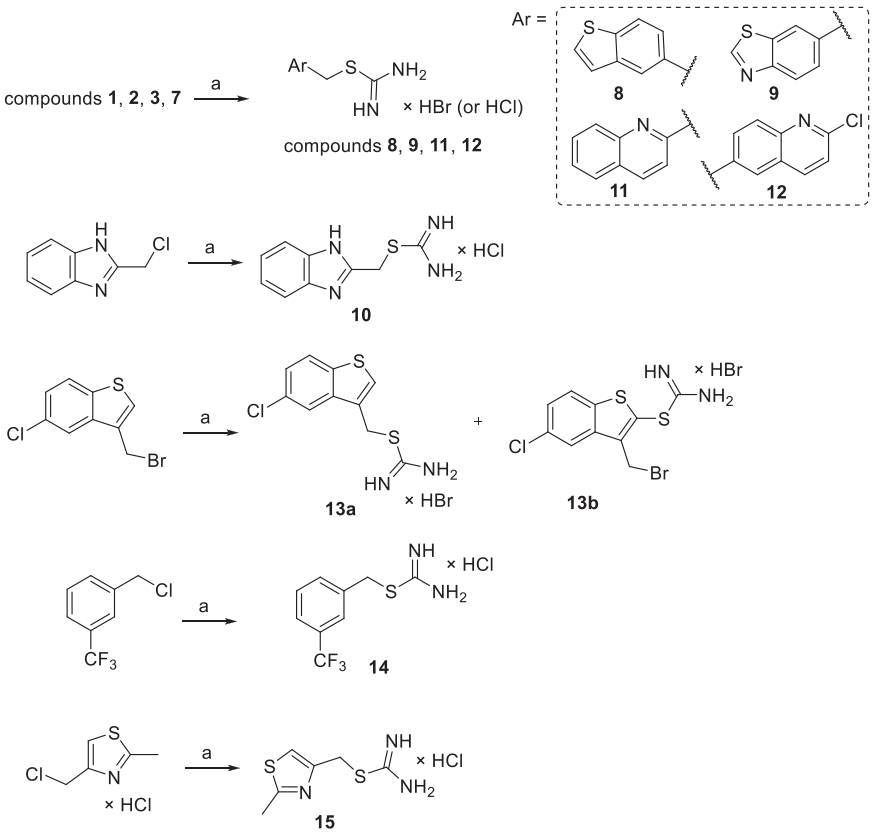

Scheme 2. Synthesis of S-substituted thiourea derivatives. Reagents and conditions: (a) thiourea, MeCN, 80 °C, 1 h, then rt, 1 h.

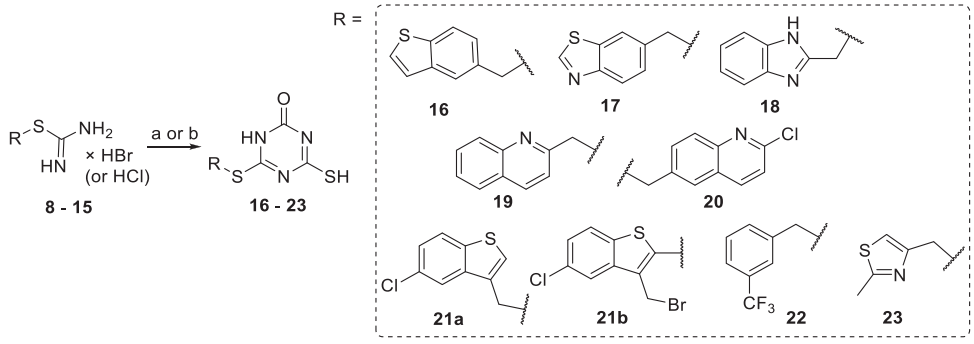

Scheme 3. Synthesis of 6-substituted 4-mercapto-1,3,5-triazin-2(1*H*)-ones. Reagents and conditions: (a) ethoxycarbonyl isothiocyanate, 2 M NaOH, toluene, H_2O, rt, 24 h; (b) ethoxycarbonyl isothiocyanate, KO*t*Bu, THF, 70 °C, 24 h (for compound **18**).

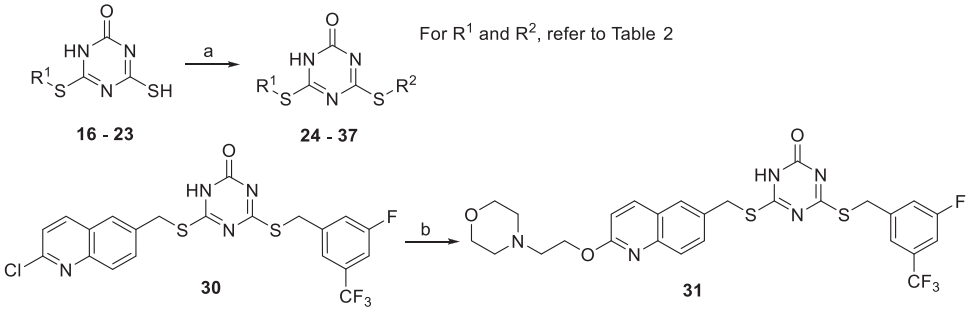

Scheme 4. Synthesis of 4,6-disubstituted-1,3,5-triazin-2(1*H*)-ones. Reagents and conditions: (a) 2 M NaOH, EtOH, rt, 2–24 h; (b) 2-morpholinoethan-1-ol, NaH, DMF, 0 °C to rt, 24 h.

2.3. Structure-activity relationship (SAR) and selectivity profiling against human protein kinases

The synthesized 4,6-substituted-1,3,5-triazin-2(*1H*)-ones **24**–**37** with novel 4,6-substituted-1,3,5-triazin-2(1*H*)-one with a 3-chlorophenyl substituent at R^1 at position 6 and etoposide as a positive control were screened for their topo IIα inhibitory activity. The results of the topo IIα-mediated decatenation assay of the tested compounds showed that all compounds exhibit favorable inhibitory properties in the same range as the previously developed compounds of this class and are superior to the clinical topo II poison etoposide (Table 2, S2-S5, Figs. S2-S4) [20,21]. Detailed data on all assays performed can be found in Sections 2, and 4 to 8 of the Supplementary material.

Model compound **31** with quinoline-based R^1 has an IC_{50} value of 18.5 ± 5.9 μM, which is as potent as our previously reported compounds that contained substituted benzyls at this position. It was encouraging to observe that compound **30**, which lacks the 2-morpholinoethoxy moiety, exhibits inhibition (IC_{50} = 12.0 ± 4.8 μM) in the same range, providing some indirect support for the *in silico* binding model where this moiety does not interact with the protein but serves to enhance solubility. Importantly, both compounds were more soluble compared to the previous series, representing an important step forward in the development of this class of compounds.

The two most active compounds of the synthesized series of compounds were **32** and **33**, both containing 5-chlorobenzo[*b*]thiophene at position 6, with IC_{50} values in the single-digit micromolar range. According to the *in silico* binding model (Fig. 2), the introduced chloro substituent on the benzo[*b*]thiophene ring can form additional favorable interactions with an empty hydrophobic pocket. The selection of substituents incorporated at position 4 of the 1,3,5-triazinone from the previous optimization study did not seem to be crucial, as molecules **24**–**26**, which all contain a benzo[*b*]thiophene substituent and either 3-trifluoromethyl-5-fluorobenzyl, 4-isopropylbenzyl, or 4-trifluoromethylbenzyl, all led to very similar topo IIα inhibition. The introduction of benzotiazole (**27**) and benzoimidazole (**28**) as bicyclic moieties was less favorable as approximately threefold lower IC_{50} values were obtained. Changing the substitution position where the quinoline was bound to the triazinone core in compound **29** had little effect on inhibition compared to compound **30** with the alternative quinoline position.

The inhibition of the compound with substituted benzyl at position 6 (compound **34**) was comparable to the compounds in which the bicyclic-type substitution pattern was installed at this position. However, this compound was less soluble and therefore less interesting for further development. Indeed, for the compounds, where a monocyclic heterocyclic thiazole was intentionally inserted to test Deepfrag's predictions, approximately three to fivefold weaker topo IIα inhibition was observed for all three resulting compounds **35**–**37** in comparison to compound **34**. Similarly, as for R^1 bicyclic compounds **24**–**26**, the choice of substitution at position 4 had little effect on the inhibitory potencies.

Next, a set of active compounds **24**, **30**, **32**, and **37** were selected to investigate whether they could inhibit the other isoform of human topo II, the β-isoform, by performing a topo IIβ-mediated decatenation assay (Table S6, Fig. S5). All compounds showed comparable inhibition to that observed for topo IIα. The average IC_{50} values were 9.9 ± 0.4 μM (compound **24**), 10.6 ± 28.8 μM (compound **30**), 8.3 ± 2.5 μM (compound **32**) and 16.0 ± 39.0 μM (compound **37**). These compounds do not appear to act selectively on topo IIα, which could be beneficial in the treatment of cancer if catalytic inhibition is involved, as the topo IIβ isoform can compensate for topo IIα depletion in certain cell lines [17,32,33].

The crystal structures of the human topo IIβ ATPase domain with bound AMP-PNP or ADP allowed a structure-based comparison of the binding sites. After structural alignment with topo IIα, it is noticeable that the positions of the crucial residues are located at the same position in both isoforms, showing a structural similarity of the ATP binding site and suggesting that selective inhibition between topo IIα and topo IIβ would be challenging when targeting this binding site. The latter is also reflected in the obtained docking modes of compounds **24** and **37**, which have the same overall orientation in both structures. In topo IIβ, Asn136 corresponds to Asn120 in topo IIα and forms hydrogen bonds with both ligands. The monocyclic and the bicyclic substituent pattern at position 6 occupy the vacant hydrophobic pocket below the ATP-adenine subpocket and interact there with Ile125 and Pro126 in topo IIα and correspondingly Ile141 and Pro142 in topo IIβ. The substituted phenyls at position 4 of the 1,3,5-triazinone are located in the ribose/phosphate part of the ATP-binding subpocket and interact with residues Ile157, Phe158, and Ala183 in topo IIβ. The same can be observed for the two compounds in topo IIα, where the corresponding residues Ile141, Phe142, and Ala167 take over this task (Fig. 4).

Finally, compounds **24**, **30**, **32**, **33** and **37** were tested to determine whether they could inhibit the topo IIα-mediated relaxation of DNA catalyzed by topo IIα. In the respective assays, overall inhibition was found to be comparable to that observed in the topo IIα-mediated decatenation assay. The IC_{50} values were 7.6 ± 2.0 μM (compound **24**), 18.1 ± 1.4. μM (compound **30**), 8.7 ± 7.3 μM (compound **32**), 7.7± 8.5μM (compound **33**) and 107.7 ± 3.8 μM (compound **37**) (Table S7, Fig. S6).

As mentioned, the physicochemical properties, particularly solubility, were generally improved in these compounds compared to the previous series. To further assess this property quantitatively, clogP values of all obtained compounds were calculated and compared to the 4,6-substituted-1,3,5-triazin-2(1*H*)-one with a 3-chlorophenyl substituent at R^1, which served as the starting point for this study (Table S29). Notably, the R^1-bicyclic compounds **27-29** and R^1-monocyclic compounds **35-37** showed lower clogP values compared to the starting compound. Interestingly, some the R1-bicyclic compounds (e.g. **24**, **30**, and **31** with included 2-morpholinoethoxy substituent) exhibited comparable clogP values to the initial compound, although they dissolved more easily during the preparation for experimental assays. This highlights the complexity of predicting solubility and indicates that often a more detailed investigation is required to fully evaluate this aspect.

Another important aspect of targeting the ATP binding site in topo IIα is the extent to which such a compound would affect human protein kinases, which are involved in the regulation of numerous processes in the cell and all contain the ATP binding site. To gain insight into the selectivity of 4,6-disubstituted 1,3,5-triazin-2(1*H*)-ones, compound **24** was tested on a panel of 20 human protein kinases (Table 3). In the group of kinases used, 9 members, CDK1/CyclinB, IGF-1R, JAK2, Flt-3, Src, PKA, PKB, Ret and FGFR3, were selected on the basis of reports on the evaluation of **QAP 1**, while the remaining 11 members were selected on the basis of studies investigating the simultaneous inhibition of topo IIα and human protein kinase(s), mainly to assess a potentially beneficial dual effect [34]. Apart from a very modest inhibition of a few kinases, no significant inhibitory effect was observed at 10 μM of the compound tested (Table 3). These results indicate that 4,6-substituted-1,3,5-triazin-2(1*H*)-ones can selectively inhibit topo IIα compared to several relevant human protein kinases.

2.4. Examining the mechanism of topo IIα inhibition

Optimization studies on 4,6-substituted-1,3,5-triazin-2(1*H*)-ones with monocyclic-based substitution at position 6 showed that they act as catalytic inhibitors. Unfortunately, sufficient quantities of the most active compounds **32** and **33** could not be obtained to perform all assays to fully investigate their mechanism of action. Therefore, a comprehensive functional evaluation of the active compounds **24** and **30** was performed. They showed comparable topo IIα inhibition and were more soluble compared to the benzyl-substituted analogues. Some of the assays were also performed for other compounds in the series such as compounds **31**, **32**, and **37**.

The topo IIα-mediated cleavage assay was carried out for compounds

Table 2
Structures of synthesized 4,6-disubstituted-1,3,5-triazin-2(1*H*)-ones and the determination of IC_{50} values by the topo IIα-mediated decatenation assay.

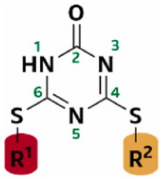

N	R^1	R^2	IC_{50} [μM]	N	R^1	R^2	IC_{50} [μM]
24	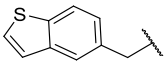	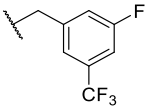	13.3 ± 1.4	**31** **	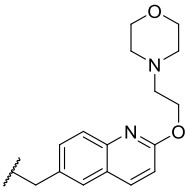	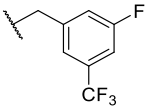	18.5 ± 5.9
25	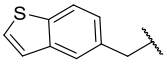	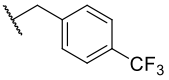	16.3 ± 0.1	**32**	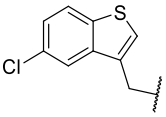	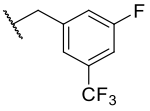	2.4 ± 1.7
26	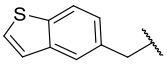	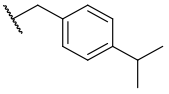	14.2 ± 1.1	**33**	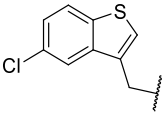	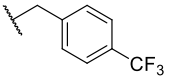	6.6 ± 1.2
27	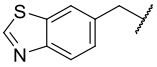	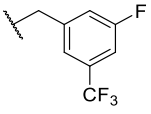	36.3 ± 5.3	**34**	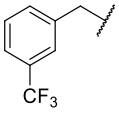	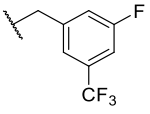	14.5 ± 11.8
28	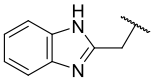	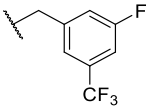	31.7 ± 3.4	**35**	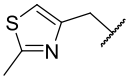	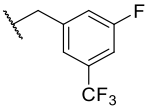	55.0 ± 6.4
29	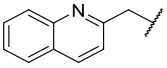	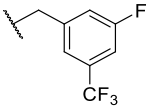	18.6 ± 6.0	**36**	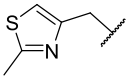	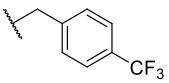	64.7 ± 6.5
30	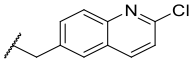	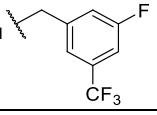	12.0 ± 4.8	**37**	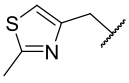	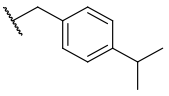	34.4 ± 6.3

* Measurements are the average of two replicates.
* * This compound is also referred to as the **model** compound, which we used in our design strategy.

24, **30**, **31**, **32**, and **37**. The **model** compound **31** showed no linear plasmid up to the measured concentration of 125 μM (Table S9, Fig. S7). For compounds **30** (Fig. 5B) and **37**, there was only a very weak increase in the linear plasmid at the highest concentration of 125 μM (Fig. S7, Table S9, S11). Based on the IC_{50} of the compounds, it can be speculated that this effect, i.e. stabilization of the cleavage complex, occurs at concentrations at which topo IIα is in principle already inhibited by binding in the ATP site. For compound **24**, a low level of linear plasmid was detected at 15.6 μM and above (Fig. 5A, S7, Table S8), whereas the amount of linear plasmid for compound **32** was higher even at lower concentrations (Fig. S7, Table S10). Thus, it appears that some members of the triazinone class may also act via another inhibitory mechanism in addition to binding to the ATP binding site at higher concentrations. This behavior varied depending on the type of substituent at position 6. This is not the first time that such behavior was observed, as chemical classes such as 2,5-disubstituted 1,3,4-thiadiazoles and α-terpyridine analogues were shown to inhibit topo II by different mechanisms, acting either as catalytic inhibitors, or as a topo II poisons, depending on very subtle changes in their substitution pattern [35–37].

The mechanism of inhibition was further investigated by performing a competitive cleavage assay for compounds **24** and **30** (Fig. 5C, S8, Table S12). The assays showed that compound **24** appeared to reduce the linear product of the etoposide-topoIIα cleavage complex at lower concentrations. However, at higher concentrations, an increase in nicked and linear DNA was observed, suggesting a DNA cleavage stabilizer (poison) effect at these concentrations. This observation is consistent with the observation in the cleavage experiment. On the other hand, compound **30** decreased the amount of linear product of the etoposide-topo IIα complex, especially at concentrations of 31.25 μM and higher, which is also consistent with the absence of a DNA cleavage stabilization (poison) effect. Further studies are needed to elucidate the additional inhibitory mechanism at higher concentrations. Studies with oligonucleotides containing the non-standard nucleobase 2-amino-imidazo[1,2-*a*]− 1,3,5-triazin-4(8*H*)-one, which showed productive

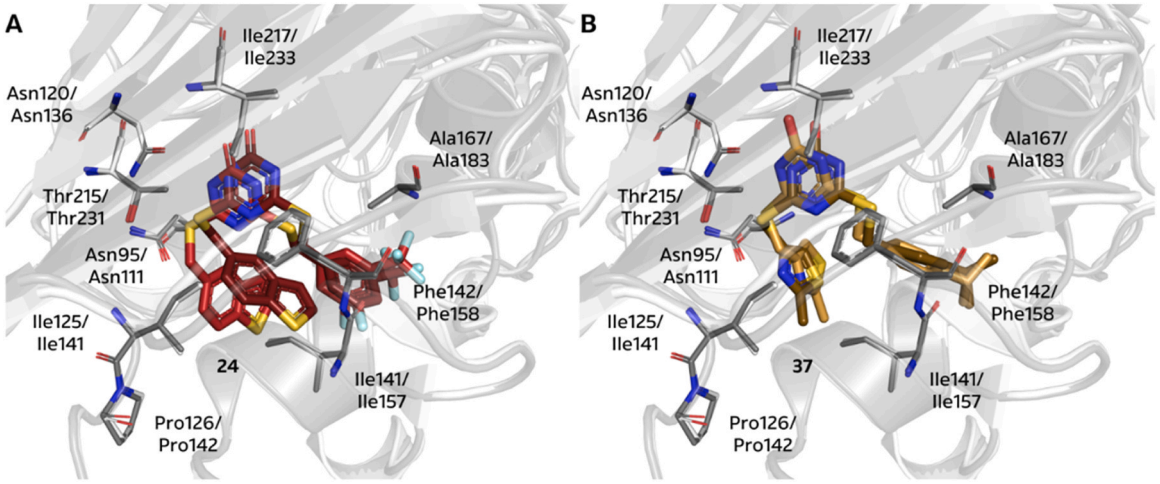

Fig. 4. Molecular docking of 4,6-disubstituted 1,3,5-triazin-2(1*H*)-ones with **(A)** bicyclic-based derivative **24** and **(B)** monocyclic-based compound **37** in the ATP binding sites of human DNA topoisomerase IIα (light) and topoisomerase IIβ (dark). The first residues belong to topo IIα, the second to topo IIβ.

Table 3
Inhibitory activity of compound **24** on a panel of human protein kinases.

Human Protein kinase	Compound 24 [% activity]
B-Raf	93
CDK1/cyclinB	124
cKit	99
c-RAF	110
EGFR	100
FGFR1	90
FGFR3	92
Flt1	93
Flt3	93
Fms	77
IGF-1R	92
JAK2	107
MEKK3	87
PDGFRα	106
PKA	86
PKBα	105
Ret	91
Src(1-530)	127
ATM	86
DNA-PK	83

binding of its moiety, similar to the triazinone core present in our compounds, to the second strand of DNA, could provide some initial clues [38].

The unwinding assay was employed to assess whether compounds **24**, **30**, and **37** act as intercalators (Fig. 5D, S9). Both etoposide and the mAMSA controls behaved as expected. Etoposide is not an intercalator and therefore showed no signs of unfolding, whereas mAMSA showed intercalator-mediated effects at all 4 concentrations with both substrates. An initial test performed with supercoiled DNA as substrate indicated that the two compounds could act as intercalators. However, when the assay was performed for the compounds with the relaxed DNA as substrate, none of the compounds showed unwinding, suggesting that they may be inhibitors of wheat germ topo I. Therefore, the assay was performed with the excess wheat germ enzyme, which showed that the compounds are indeed inhibitors rather than intercalators, with compound **24** being the most potent. These observations are consistent with the earlier assays.

The mode of action of **24** and **30** was also investigated using the competitive ATPase assay to discern how 4,6-disubstituted-1,3,5-triazin-2(1*H*)-ones influence ATP hydrolysis at varying concentrations of the ATP molecule. The results are presented in the form of graphs of ATP hydrolysis rates as a function of increasing ATP concentrations (Fig. 6, S10, Tables S13, S14). For both inhibitors, the ATP hydrolysis rate was significantly faster at lower concentrations and then slowed down with increasing concentration of the compounds, showing a significant concentration-dependent effect on ATP hydrolysis rate. Since the inhibition of ATP hydrolysis with **24** was very strong at high concentrations, the assay was adjusted to lower concentrations of the compound. In addition, the IC_{50} values of **24** and **30** were calculated with respect to ATP (Table S15). For compound **30**, a general trend of decreasing IC_{50} values with decreasing ATP concentration (up to 0.1 mM ATP) was observed, which indicates ATP-competitive inhibition. For compound **24**, there was no noticeable decrease in IC_{50} values, so no conclusions could be drawn: however, this suggests a possible additional inhibitory mechanism, consistent with the other assays.

2.5. Binding model of triazinones to the ATP binding site: Integrating in silico insights with STD NMR experiments

The only experimental data on the binding of 4,6-substituted-1,3,5-triazin-2(1*H*)-ones to the ATP binding site of topo IIα was a microscale thermophoresis (MST) experiment, which showed that these compounds bind to this domain. In this study, the *in silico* binding model derived for this class [20,21], was further indirectly supported by the results of the topo IIα inhibition data for compounds **30** and (**model**) **31**. The results demonstrated that the introduction of a large 2-morpholinoethoxy group to the R^1 quinolin-6-yl substituent with the aim of improving solubility in **31** had little effect on the overall inhibitory potency. To further explore the binding of this class of compounds and corroborate the model, the interaction between several triazinones and the isolated ATPase domain of topo IIα was investigated with ^{1}H saturation transfer difference (STD) NMR experiments [39], which confirmed the interaction of compounds **30** and (**model**) **31** with the ATPase domain of topo IIα.

To determine the ligand-enzyme contacts more precisely, 1D ^{1}H STD epitope mapping revealed the involvement of the protons of the 2-substituted quinolin-6-yl ring (position 6) as well as the 3-fluoro-5-(trifluoromethyl)benzyl (position 4) of **30** in the interaction with the ATPase domain. In our *in silico* binding model, this was reflected in the hydrophobic interactions observed when these moieties interacted with residues such as Ile142, Phe142 and Ile125, Pro126 (Fig. 7A, S12). A similar result was observed in the epitope mapping of **model** compound **31**. For this molecule, where the chlorine of **30** was replaced by morpholinoethoxy, a slight decrease in STD effects was observed for protons of the 2-substituted quinolin-6-yl ring compared to 3-fluoro-5-

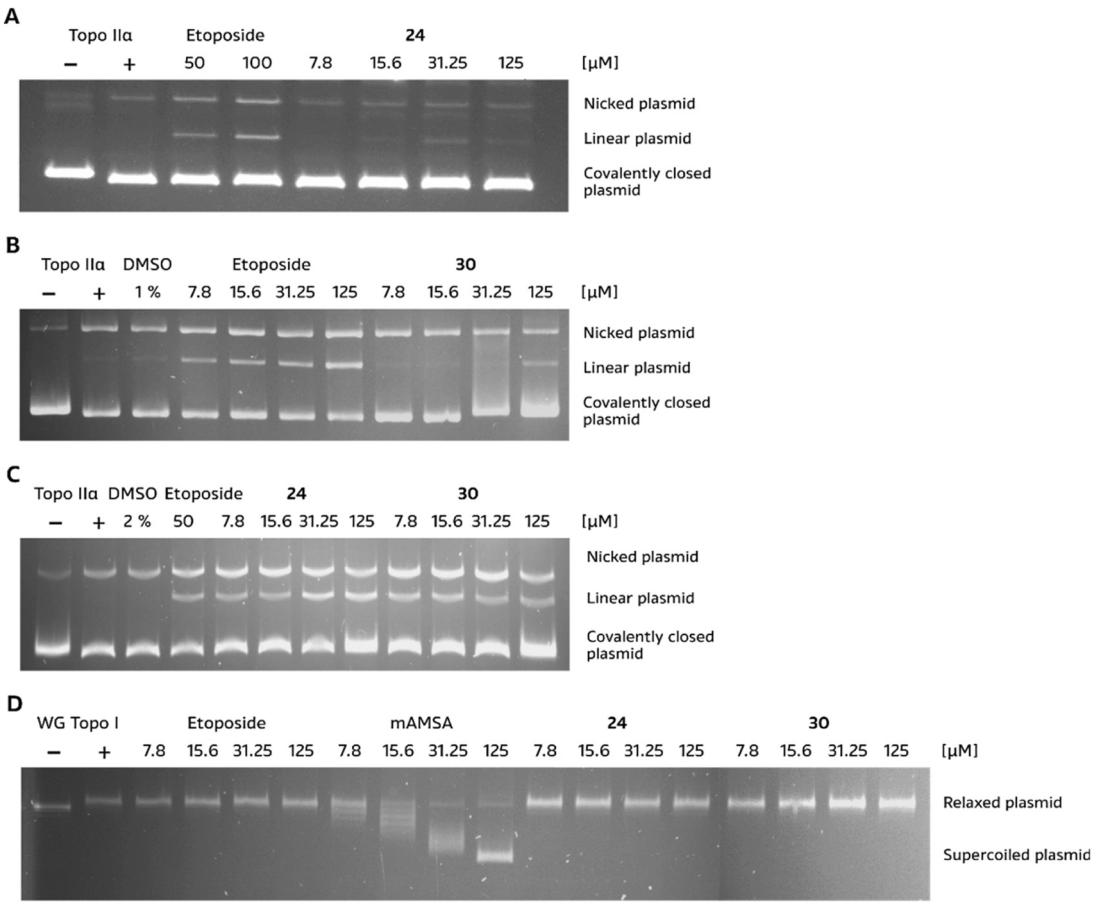

Fig. 5. Functional assays of the selective 4,6-substituted-1,3,5-triazin-2(1*H*)-ones **24** and **30.** (**A**) Topo IIα-mediated cleavage assay for **24** and etoposide as positive control. (**B**) Topo IIα-mediated cleavage assay for **30** and etoposide as positive control. (**C**) Human topo IIα competitive cleavage assay was performed with 4 different concentrations of compounds **24** and **30** in the presence of 50 μM etoposide. (**D**) Unwinding assay for **24** and **30** and intercalator *m*-AMSA as positive control.

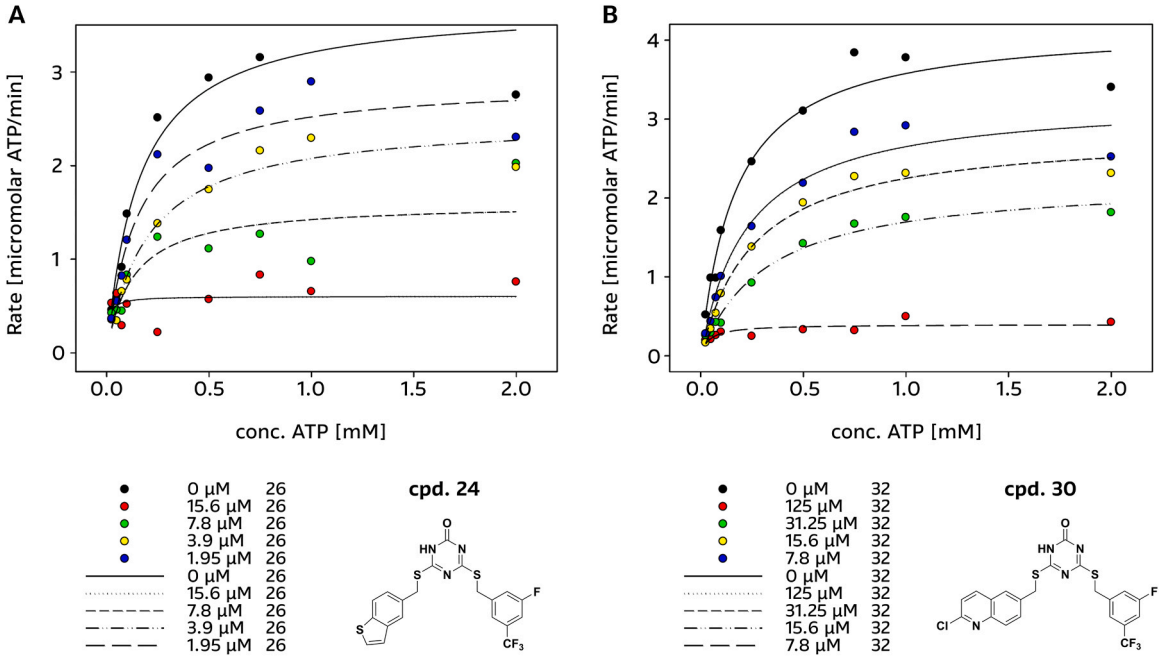

Fig. 6. Results of the competitive ATPase assay shown as plots of the ATP hydrolysis rates versus the ATP concentrations used together with different concentrations of 4,6-substituted 1,3,5-triazin-2(1*H*)-ones, (**A**) compound **24** and (**B**) compound **30**.

(trifluoromethyl)-benzyl (Fig. 7B, S13). It should be noted that the strength of the interactions with the protein under study can only be compared between atoms within a given molecule, as the magnitude of the STD amplification factor also depends on the exchange kinetics of the ligand. Overall, the STD NMR data provided a further rationalization of the binding mode of 4,6-substituted-1,3,5-triazin-2(1*H*)-ones suggested by *in silico* experiments.

To further investigate the binding dynamics of optimized 4,6-disubstituted-1,3,5-triazin-2(1*H*)-one, STD NMR experiments with compound **24** bearing benzo[*b*]thiophen-5-yl ring at position 6 were performed, which had been investigated extensively in functional topo IIα assays. STD NMR confirmed the interaction of compound **24** with the ATPase domain and showed a slight increase in STD effects observed for protons of the benzo[*b*]thiophen-5-yl ring compared to the 3-fluoro-5-(trifluoromethyl)-benzyl moiety, suggesting that this ring binds more favorably compared to the 2-substituted quinolin-6-yl in compounds **30** and **31** (Figs. 8B, 8E, S14).

The docking binding mode of compound **24** was also subjected to computational evaluation in a 0.5 μs MD simulation. The average RMSD of the ligand was 3.1 ± 0.4 Å, which is in the same range as compounds **31** and **QAP 1** (Fig. 8A). The dynophore model shows favorable hydrophobic interactions between the R^1 benzo[*b*]thiophene moiety and residues Ile125 and Thr159, which are part of the vacant hydrophobic pocket below the adenine moiety, and with Thr215. The 3-fluoro-5-(trifluoromethyl)-benzyl interacted with residues Ile141, Tyr151, and Ala167 in the phosphate sub-pocket. The simulation results were in general agreement with the STD NMR results and were also comparable with the observations of **model** compound **31**. As expected, **24** formed hydrogen bonds with Asn120, in this case mainly with the sulfur atom at substitution position 6 of the 1,3,5-triazin-2(1*H*)-one scaffold, stably placed near this residue. The remaining hydrogen bonds were mainly formed between the trifluoromethyl substituent at position 4 and

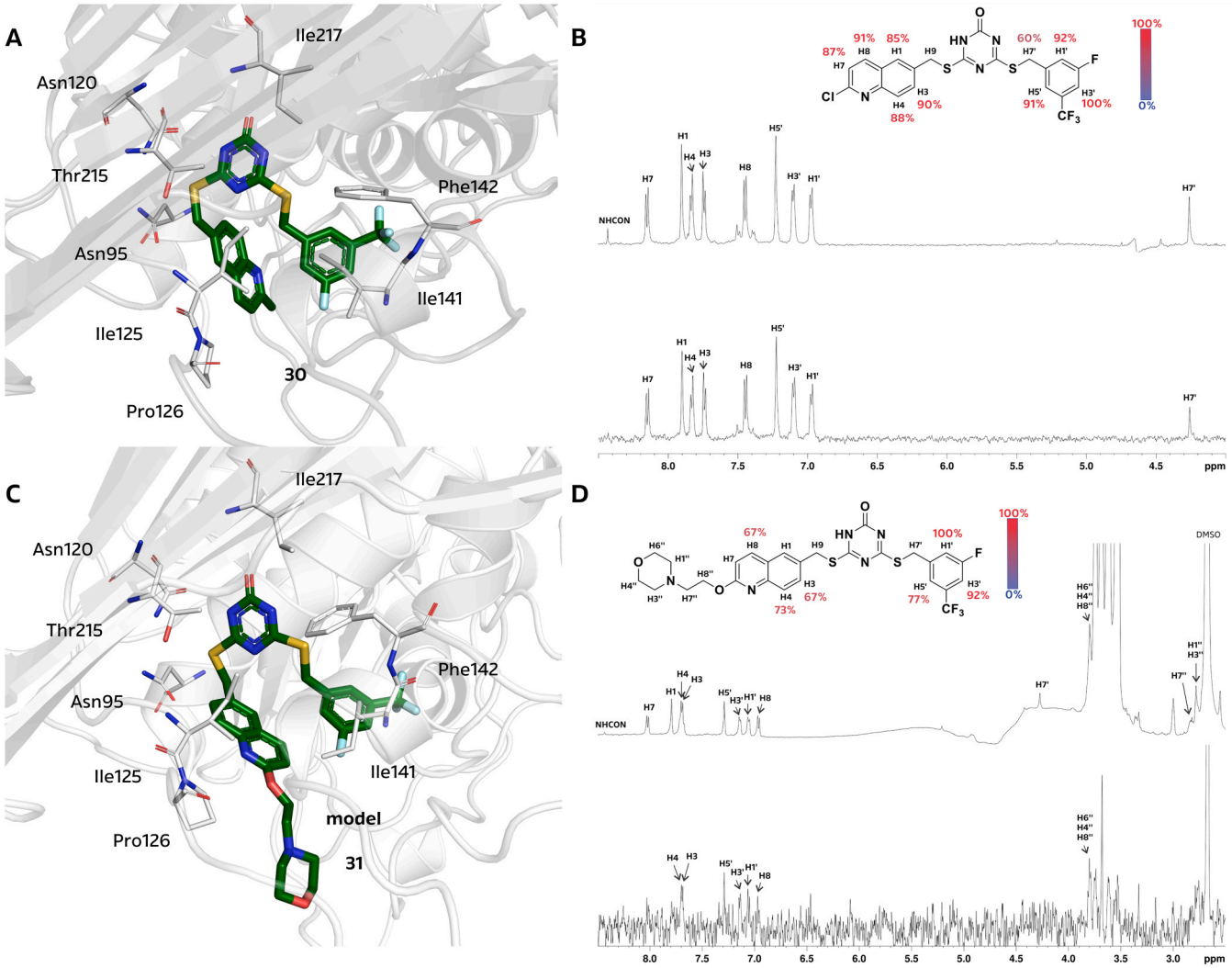

Fig. 7. (**A, C**) *In silico* binding modes of compounds **30** and **31** in the ATP binding site of topo IIα. (**B**) 1D ^{1}H STD NMR spectra for compound **30** recorded at a topo IIα ATPase domain: compound **30** ratio of 1:100 and 600 MHz. The molecular structure illustrates the proton nomenclature and the color-coded relative degrees of saturation of the individual non-overlapping protons. The STD amplification factors were normalized to the intensity of the signal with the largest STD effect. The reference STD spectrum (top) with proton assignment and the difference STD spectrum (bottom) are shown. The signal for H9 is missing in the spectra due to interference from water suppression. The spectra are not to scale. (**D**) 1D ^{1}H STD NMR spectra for compound **31** recorded at a topo IIα ATPase domain: compound **31** ratio of 1:100 and 600 MHz. The molecular structure illustrates the proton nomenclature and the color-coded relative degrees of saturation of the individual non-overlapping protons. The STD amplification factors were normalized to the intensity of the signal with the largest STD effect. The reference STD spectrum (top) with proton assignment and difference STD spectrum (bottom) are shown. The signal for H9 is missing in the spectra due to interference from water suppression. Since the signals for H4″, H6″ and H8″ overlap with signals belonging to the protein buffer with glycerol, their STD amplification factors could not be determined. The intensities of H1, H7, H7′, H1′, H3′ and H7′ are under detection limit in the difference STD spectrum. The spectra are not to scale.

residues Ser148, Ser149, and Asn150 (Fig. 8C-D). The free energy decomposition (per residue) again revealed that Asn120 has the strongest interaction, which is again weaker than in the case of **QAP 1**. MM/GBSA identified that Ile125 and Thr215 contribute favorably to the binding of benzo[*b*]thiophene. As with the R^2 substituent, the interaction with Ile141 proved to be particularly important from an energetic point of view. In addition, several other residues such as Ile88, Asn91, Ala92, Asn95, Pro126, Phe142, and Ile217 also proved to be important and were not included in the dynophore (Fig. 8F). This necessitates the integration of dynophore and MM/GBSA approaches when attempting to comprehensively understand the binding of a compound. Subsequent integration of these *in silico* results with STD NMR experiments was critical in confirming the catalytic inhibition mode of **24** by inhibiting topo IIα via binding to the ATP site. However, the cleavage and competitive cleavage experiments performed indicated that **24** can stabilize the cleavage complex at higher concentration. Further studies

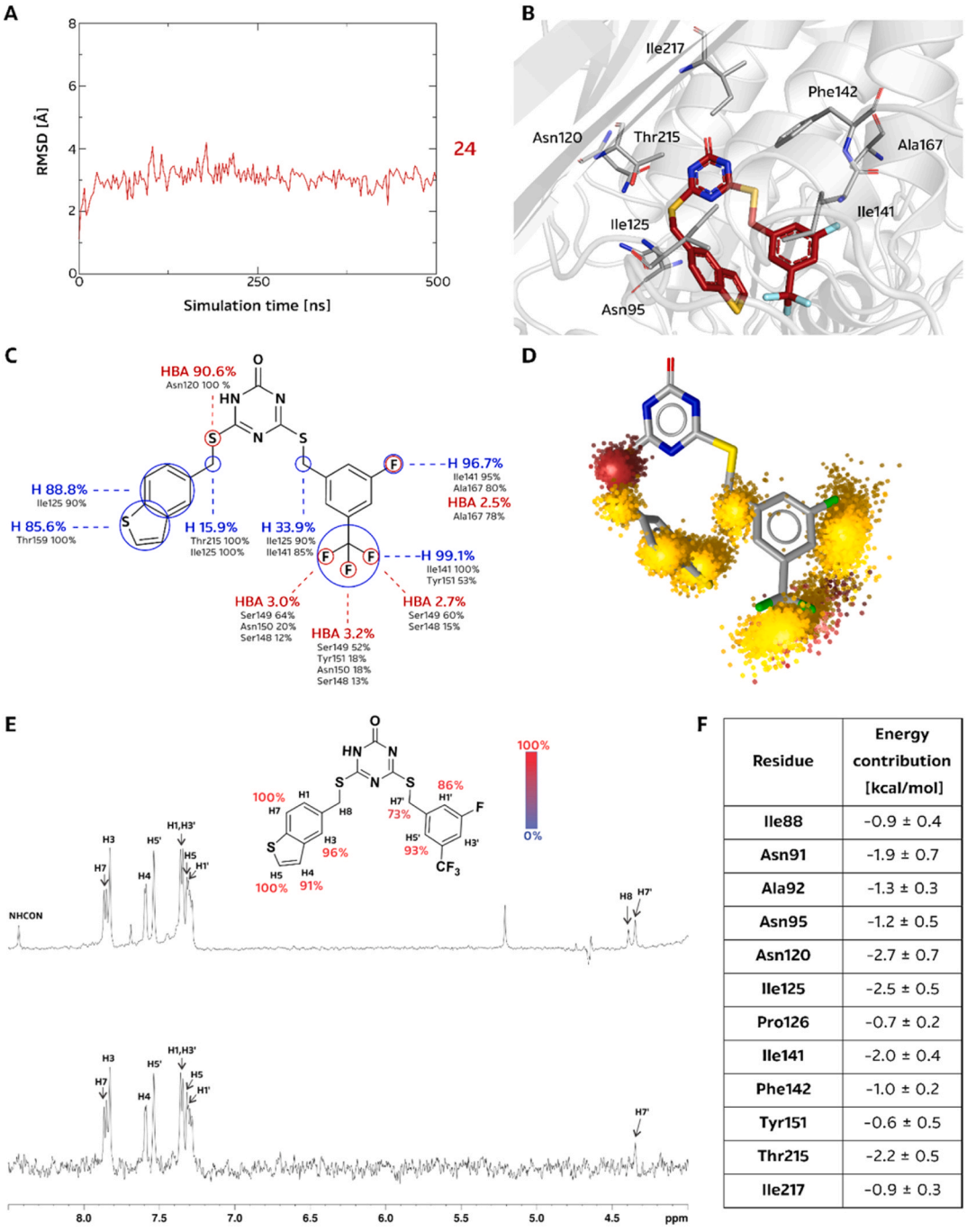

Residue	Energy contribution [kcal/mol]
Ile88	-0.9 ± 0.4
Asn91	-1.9 ± 0.7
Ala92	-1.3 ± 0.3
Asn95	-1.2 ± 0.5
Asn120	-2.7 ± 0.7
Ile125	-2.5 ± 0.5
Pro126	-0.7 ± 0.2
Ile141	-2.0 ± 0.4
Phe142	-1.0 ± 0.2
Tyr151	-0.6 ± 0.5
Thr215	-2.2 ± 0.5
Ile217	-0.9 ± 0.3

Fig. 8. (**A**) RMSD of compound **24**. (**B**) MD snapshot of compound **24** (dark red) in the ATP binding site (grey). (**C**) 2D scheme of the dynophore model and (**D**) 3D dynophore model. (**E**) 1D ^{1}H STD NMR spectra for the compound **24** recorded at a topo IIα ATPase domain: compound **24** ratio of 1:100 and 600 MHz. The molecular structure illustrates the proton nomenclature and the color-coded relative degrees of saturation of the individual non-overlapping protons. The STD amplification factors were normalized to the intensity of the signal with the largest STD effect. The reference STD spectrum (top) with proton assignment and the difference STD spectrum (bottom) are shown. The signal for H8 is missing in the reference spectrum due to interference from water suppression. The spectra are not to scale. (**F**) Per-residue decomposition of the binding free energy of compound **24** with residues with which the compound interacts most favorably.

are therefore required to decipher this inhibitory mechanism, which is more or less pronounced depending on the substitution pattern of the member of this chemical class.

Compound **37** with the monocyclic R^1 substituent 2-methylthiazole was also of interest for investigation, and STD NMR experiments confirmed its interaction with the ATPase domain. Compound **37** exhibited uneven degrees of saturation of the individual protons, with the STD effect of the methylene and methyl groups being much lower compared to the aromatic rings, suggesting that these groups have weaker interactions with the binding site than the rest of the molecule. The highest degree of saturation was interestingly observed for the proton H1 of the thiazole ring. The replacement of 2-methylthiazole and 4-isopropylbenzyl in compound **37** with 3-fluoro-5-(trifluoromethyl) benzyl and 2-substituted quinolin-6-yl or benzo[*b*]thiophen-5-yl rings in compounds **24, 30**, and **31** unified the STD effects of the aromatic moieties in these molecules, indicating a stronger interaction of all three compounds with the binding site compared to compound **37**, which is consistent with the observed difference in topo IIα inhibition (Fig. S11, S15). Additional information regarding the ^{1}H chemical shifts of assigned protons and STD amplification factors can be found in the Supplementary Information in Section 9.

The binding mode of compound **37** was also investigated in molecular simulations. The average RMSD of the ligand was 2.6 ± 0.5 Å, which shows that it is stably bound (Fig. S18A). The hydrogen bond interactions between Asn120 with 1,3,5-triazin-2(1*H*)-one and the linker sulfur atom at substitution site 6 were again energetically the strongest. In addition to the interactions between the substituents at positions 4 and 6 and the hydrophobic residues already identified and described for previous compounds, an additional aromatic interaction with the residue Arg98 was discovered using dynophore analysis, which could explain the strong STD effect observed for the proton H1 of the thiazole ring. Upon visualization of the trajectory, Arg98 was positioned orthogonal to the aromatic ring, but its guanidine moiety was positioned parallel to the thiazole ring, forming a cation-π interaction (Fig. S18B - D). Overall, integration of dynophore and MM/GBSA data was again central for a comprehensive analysis of triazinone binding properties (Table S24).

2.6. Optimizing cancer targeting through NCI-60 screening: Identifying sensitive human cancer cell lines for future compound class development

The 4,6-substituted-1,3,5-triazin-2(1*H*)-ones with bicyclic- (**24**, **25**, and **26**) and monocyclic-based (**34** and **37**) substituents at position 6 were submitted to the National Cancer Institute (USA), where they were approved for NCI-60 screening. This comprehensive assay was performed on a set of 60 human cancer cell lines ranging from leukemia, lung, colon and central nervous system cancer, melanoma, ovarian, kidney, prostate and breast cancer, providing a good insight into their overall potential for development as anticancer agents. A closer look at the growth inhibition levels allows the identification of human cancer cell lines in which these compounds were cytotoxic. This data may provide a good starting point for further steps in the anticancer drug discovery pipeline using this class of compounds.

In general, the compounds with R^1 bicyclic substituents performed better in NCI-60 than the monocyclic-based triazinones. Compounds **34** and **37** with monocyclic-based substitution pattern at position 6 did not exhibit cytotoxic activity (Fig. 9C and Fig. S20). Compound **24** showed marginal cytotoxicity in several leukemia cell lines as well as in some

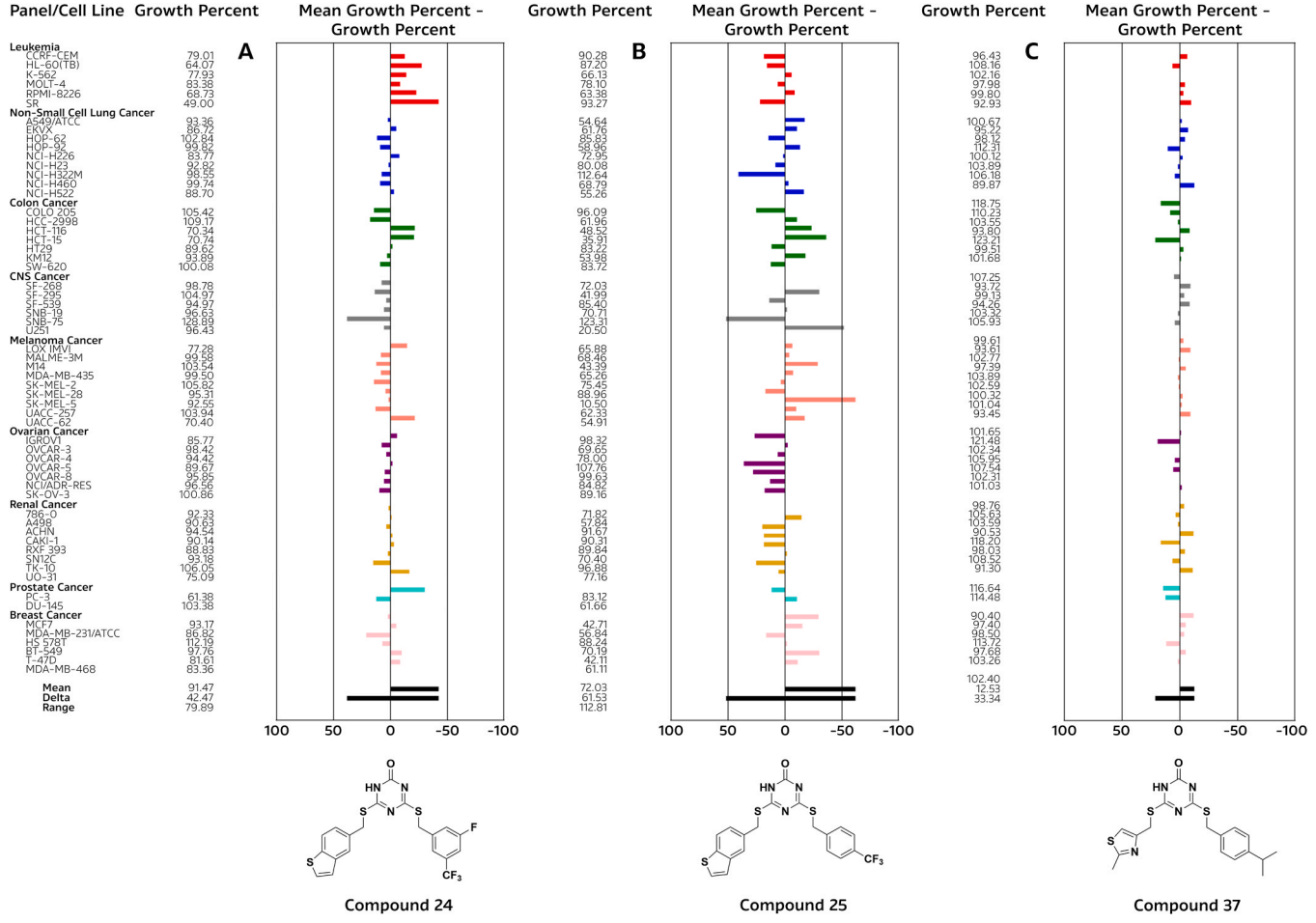

Fig. 9. Cytotoxicity of compounds (A) **24, (B) 25**, and (C) **37** were tested using a 10 μM concentration on a panel of NCI-60 human cancer cell lines.

colon cancer, melanoma and prostate cancer cell lines (Fig. 9A). Interestingly, the structurally closely related compound **25** with para-substituted CF_3-benzyl moiety showed more diverse and potent cytotoxic effects on a broader spectrum of cancer cell lines. While it also showed cytotoxicity on leukemia cell lines, the most sensitive cell lines were the malignant glioblastoma cell line U251 (80 % inhibition of cell growth) and the malignant melanoma cell line SK-MEL-5 (89.5 % inhibition of cell growth). In addition, several cancer cell lines were observed in which cell growth was reduced by 50 % or more. These cell lines belong to colon (colorectal adenocarcinoma, colorectal carcinoma and colon adenocarcinoma) and breast cancer (breast adenocarcinoma) (Fig. 9B). Admittedly, compound **25** has not been studied as extensively as compound **24**, but based on the close structural similarity, we can infer its mode of action on topo IIα and molecular recognition from the behavior observed for **24**. For compound **26** (Fig. S19), the cytotoxic activity was much lower compared to **24** and **25**. This could indicate the importance of the CF_3 group, as compound **26** contains an isopropyl substituent. As the NCI is currently not accepting submissions of compounds outside of US for the NCI-60 screening, a later submission of compounds **30** and **31** was not possible. The results collected on the human cell lines indicate that leukemia, glioblastoma, and breast cancer are the most promising cancer types to focus on for future development. Topo IIα is widely expressed in skin, bone marrow, lymphoid tissue, lymph nodes, tonsils, and male and female tissues [40–44]. The sensitivity observed in the NCI-60 screening therefore corresponded well with the desired preclinical development for agents targeting topo IIα.

3. Conclusion

In our efforts to develop 4,6-substituted-1,3,5-triazin-2(1*H*)-one derivatives as inhibitors of human DNA topo IIα targeting the ATP binding site, we focused on optimizing the R^1 substitution pattern at position 6. Inspired by the binding of preclinical 9*H*-purine derivative **QAP 1**, we incorporated bicyclic substituents at this position and used molecular simulations to validate the advantages of this modification. Since Deepfrag, a specialized deep learning software tailored for structure-based lead optimization, suggested a preference for monocyclic-based substituents, we pursued a dual approach. We synthesized both bicyclic and monocyclic substituents at position 6 of the 1,3,5-triazin-2(1*H*)-one scaffold, the latter specifically to validate the Deepfrag predictions.

The SAR of the triazinones showed that the bicyclic-substituted triazinones exhibited comparable inhibition of topo IIα to their monocyclic counterparts, accompanied by an overall improved solubility. The introduction of the additional morpholino group to improve solubility did not have a detrimental effect on inhibition, indirectly confirming the *in silico* binding model. The comparatively lower inhibitory activity of the compounds with heteromonocyclic substituents at position 6 served as initial crude positive validation of the Deepfrag predictions. The compounds inhibited the topo IIβ isoform equally strongly, which is favorable since the compounds mainly act as catalytic inhibitors. Evaluation on a panel of 20 human protein kinases showed selectivity towards inhibition of topo IIα.

Mechanistic studies showed that compounds are predominantly catalytic inhibitors, although some of them can act as topo II poisons at higher concentrations. The extent of this effect depended on subtle structural changes that were already observed with other topo IIα inhibitors. STD NMR experiments confirmed the interaction of the compounds with the isolated ATPase domain and provided additional evidence for catalytic inhibition by ATP binding. However, further studies are required to elucidate the additional inhibitory mechanism at higher concentrations. Integration of STD NMR epitope mapping with molecular simulations, dynamic pharmacophore modeling, and MM/GBSA free energy calculations provided further evidence for the derived triazinone binding model, with the Asn120 interaction being the strongest contributor to binding, in addition to engagement of substituents at positions 4 and 6 via hydrophobic interactions with the binding site. Since the substituent at position 6 occupies a vacant hydrophobic region outside the ATP-binding pocket, this could be a potentially crucial factor for selective binding.

The NCI-60 screening showed a higher cytotoxicity of compounds with the bicyclic substitution at position 6, which further supports the development in this direction. The identification of sensitive human cancer cell lines, in particular glioblastoma, breast cancer and leukemia, underlines the translational relevance of our results for further preclinical development of this class of compounds. Finally, this study is also an example of the synergy between simulation and AI-based approaches to efficiently guide molecular design in drug optimization.

4. Experimental section

4.1. General chemistry information

Reagents and solvents were used as received from commercial suppliers (Acros Organics, Aldrich, TCI Europe, Merck, Alfa Aesar, Fluorochem). For reactions involving air or moisture sensitive reagents, solvents were distilled before use (e.g. THF) and these reactions were carried out under argon atmosphere. Reactions were monitored using analytical thin-layer chromatography on Silica gel 60 F_{254} Al plates (20 × 20 cm, Merck, Germany). Developed plates were inspected under UV light and visualized with ninhydrin, $FeCl_3$, or bromocresol green stains. Normal phase flash column chromatography was performed on Silica gel 60 (particle size: 0.035–0.070 mm, Merck).

Nuclear magnetic resonance (NMR) spectra were recorded on a Bruker Avance III 400 MHz spectrometer at 400 MHz for ^{1}H, 101 MHz for ^{13}C, respectively, using DMSO-d_6, $CDCl_3$, acetone-d_6, and CD_3OD as solvents. Chemical shifts are reported in *parts per million* (*ppm*), and are referenced to the deuterated solvent used, i.e., for $CDCl_3$ at 7.26 ppm for ^{1}H and 77.16 ppm for ^{13}C, for DMSO-d_6 at 2.50 ppm for ^{1}H and 39.52 ppm for ^{13}C, for acetone-d_6 at 2.05 ppm for ^{1}H and 29.84 ppm for ^{13}C, and for CD_3OD at 3.31 ppm for ^{1}H and 49.00 ppm for ^{13}C. The multiplicities are reported as s (singlet), d (doublet), t (triplet), q (quartet), p (pentet), m (multiplet), dd (doublet of doublets), ddd (doublet doublet of doublets), td (triplet of doublets), qd (quartet of doublets), and br (broad), and coupling constants (*J*) in Hertz (Hz).

Mass spectra and high-resolution mass measurements were recorded on a Thermo Scientific Q Exactive Plus mass spectrometer (Thermo Fisher Scientific, Waltham, MA, USA). LC-MS measurements were performed on an Agilent Infinity 1260 (Santa Clara, CA, USA). A C18 column was used (Waters xBridge BEH; 4.6 mm × 150 mm, 3.5 μm) at 40 °C. The flow rate was of the mobile phase was 1.5 mL/min, the injection volume was 10 μl, and the products were detected at 254 nm. Solvent A comprised 1 % MeCN and 0.1 % HCOOH in double-distilled H_2O; Solvent B comprised MeCN. The following elution gradient was used: 0→1 min, 25 % B; 1→6 min, 25 %→98 % B; 6→6.5 min, 98 % B; 6.5→7 min, 98 %→25 % B; 7→10 min, 25 % B. UHPLC analyses were performed on a Thermo Scientific Dionex UltiMate 3000 modular system (Thermo Fisher Scientific), equipped with a photodiode array detector set to 254 nm. A Waters Acquity UPLC® HSS C18 SB column (1.8 μm, 2.1 mm × 50 mm) was used, thermostated at 40 °C. The mobile phase consisted of 0.1 % TFA in H_2O (A) and MeCN (B), employing the following gradient: 95 % A to 5 % A in 10 min, then 95 % B for 4 min, with flow rate of 0.3 mL/min and injection volume of 5 μl. The purities of the final compounds used for the biological evaluations were ≥ 95 %, unless stated otherwise.

4.1.1. General procedure for bromination

To a solution of a methylated heterocycle (1.0 equiv.) in CCl_4 (5 mL for 1.0 mmol of the starting compound) or benzene (8 mL for 1.0 mmol of the starting compound), NBS (from 0.95 to 2.0 equiv.) and DBPO (0.05 equiv.) were added. The reaction mixtures were stirred at different temperatures and the reaction time was also varied (see details next to each compound). After the reaction was complete, the volatiles were

removed under reduced pressure and the crude residues were either used in the next step or purified by column chromatography.

4.1.2. General procedure for the preparation of thiourea derivatives

To a solution of the appropriate alkyl halide (1.0 equiv.) in MeCN (5 mL for 1.0 mmol of the starting compound), thiourea (1.3 equiv.) was added and the mixture first stirred at 80 °C for 1 h, followed by stirring at rt for additional 2 h. The resulting suspension was filtered off, washed with cold (0 °C) MeCN, and dried. This process yielded pure compounds **8–16**.

4.1.3. General procedure for the synthesis of 6-substituted 4-mercapto-1,3,5-triazin-2(1 H)-ones

To a solution of the appropriate thiourea derivative (l.0 equiv.) in H_2O (4 mL for 1.0 mmol of the thiourea analog), toluene (4 mL for 1.0 mmol of thiourea analog) was added and the mixture stirred vigorously for 5 min. Then, ethoxycarbonyl isothiocyanate (1.4 equiv.) in toluene (2 mL for 1.0 mmol of ethoxycarbonyl isothiocyanate) and NaOH (2 M, 1 mL for 1.0 mmol of thiourea analog) were simultaneously added over a period of 5 min. Additional NaOH (2 M, 2 mL for 1.0 mmol of thiourea analog) was added after 15 min and the reaction mixture was stirred at rt for 24 h. After the reaction was complete, toluene (30 mL) and NaOH (2 M, 30 mL) were added to the mixture. The phases were then separated and the alkaline phases were acidified to pH 1 with H_2SO_4 (2 M). The precipitate was formed, which was then filtered off, washed with *n*-hexanes, and purified (see details next to each compound).

4.1.4. General procedure for the synthesis of 4,6-disubstituted-1,3,5-triazin-2(1H)-ones

To a solution of the appropriate 6-substituted 4-mercapto-1,3,5-triazin-2(1*H*)-one (1.0 equiv.) in EtOH (4 mL for 1.0 mmol of the starting compound) and NaOH (2 M, 2 mL for 1.0 mmol of the starting compound), the corresponding benzyl halide (l.1 equiv.) was slowly added. The reaction mixture was stirred at rt for 2 h. After the reaction was complete, H_2O (4 mL for 1.0 mmol of the starting compound) was added, followed by the addition of H_2SO_4 (2 M, until pH value reached 1). The precipitate was formed, which was then filtered off, and purified additionally if needed (see details next to each compound).

4.1.5. Synthesis of brominated compounds

4.1.5.1. 5-(Bromomethyl)benzo[b]thiophene (1) [45]. The reaction was carried out according to the General procedure for bromination, starting from 5-methylbenzo[*b*]thiophene (148 mg, 1.00 mmol), NBS (169 mg, 0.95 mmol), and dibenzoyl peroxide (12 mg, 0.05 mmol) in CCl_4. The mixture was first heated at 80 °C for 2 h, followed by stirring at rt for 16 h. After evaporation, compound **1** (159 mg, 70 % yield) was isolated as a brown solid, which was used in the next step without further chromatographic purification. Spectroscopic data were identical to those reported previously [45]. R_f: 0.44 (EtOAc/*n*-hexanes 1/9); ^{1}H NMR (400 MHz, $CDCl_3$) δ 4.65 (s, 2 H, CH_2), 7.32 (dd, J_1 = 4.4 Hz, J_2 = 0,5 Hz, 1 H, Ar-*H*), 7.38 (dd, J_1 = 8.4 Hz, J_2 = 1.7 Hz, 1 H, Ar-*H*), 7.48 (d, J = 5.5 Hz, 1 H, Ar-*H*), 7.83–7.87 (m, 2 H, Ar-*H*); HRMS (ESI) *m/z* calcd for C_9H_8BrS $[M+H]^+$ 226.9457, found 226.9455.

4.1.5.2. 6-(Bromomethyl)benzo[d]thiazole (2) [46]. The reaction was carried out according to the General procedure for bromination, starting from 6-methylbenzo[*d*]thiazole (900 mg, 6.03 mmol), NBS (2.15 g, 12.1 mmol), and dibenzoyl peroxide (146 mg, 0.60 mmol) in CCl_4. The mixture was stirred at rt for 4 h. Compound was purified by column chromatography using acetone/*n*-hexanes (1/5) as an eluent system to give **2** (591 mg, 43 % yield) as a brown solid. Spectroscopic data were identical to those reported previously [46]. R_f: 0.23 (acetone/*n*-hexanes 1/5); ^{1}H NMR (400 MHz, DMSO-d_6) δ 4.87 (s, 2 H, CH_2), 7.62 (dd, J_1 = 8.4 Hz, J_2 = 1.8 Hz, 1 H, Ar-*H*), 7.82 (dd, J_1 = 8.6 Hz, J_2 = 1.9 Hz, 1 H, Ar-*H*), 8.28 (d, J = 1.6 Hz, 1 H, Ar-*H*), 9.43 (s, 1 H, Ar-*H*); HRMS (ESI) *m/z* calcd for C_8H_7BrNS $[M+H]^+$ 227.9408, found 227.9411.

4.1.5.3. 2-(Bromomethyl)quinoline (3) [47]. To a solution of 2-methylquinoline (1.43 g, 10 mmol, 1.0 equiv.) in MeCN (20 mL), CuBr (2.15 g, 15 mmol, 1.5 equiv.) and TBHP (70 %, 11.0 mL, 80 mmol, 8.0 equiv.) were added. The reaction mixture was stirred at 70 °C overnight. Then, H_2O (100 mL) was added and the mixture washed with CH_2Cl_2 (3 × 100 mL). The combined organic phases were washed with $Na_2S_2O_3$ (40 mL) and NH_4Cl (160 mL), dried with Na_2SO_4, filtered, and the solvent evaporated to give the crude product. Compound **3** was purified by column chromatography using EtOAc/*n*-hexanes (1/15) as an eluent system. Spectroscopic data were identical to those reported previously [47]. Brown solid; yield, 14 % (308 mg); R_f: 0.40 (EtOAc/*n*-hexanes 1/7); ^{1}H NMR (400 MHz, DMSO-d_6) δ 4.86 (s, 2 H, CH_2), 7.63 (ddd, J_1 = 8.7 Hz, J_2 = 7.0 Hz, J_3 = 1.2 Hz, 1 H, Ar-*H*), 7.68 (d, J = 8.4 Hz, 1 H, Ar-*H*), 7.79 (ddd, J_1 = 8.7 Hz, J_2 = 6.9 Hz, J_3 = 1.5 Hz, 1 H, Ar-*H*), 7.96–8.02 (m, 2 H, Ar-*H*), 8.41 (d, J = 8.4 Hz, 1 H, Ar-*H*); HRMS (ESI) *m/z* calcd for $C_{10}H_9BrN$ $[M+H]^+$ 221.9839, found 221.9834.

4.1.5.4. Procedure for the preparation of compound 6. To a solution of cinnamic acid (1.4 g, 10.0 mmol, 1.0 equiv.) in toluene (10 mL), $SOCl_2$ (7.3 mL, 11.9 g, 100 mmol, 10.0 equiv.) was added slowly. The reaction mixture was stirred at 80 °C for 2 h, followed by evaporation of volatiles under reduced pressure. The residue was dissolved in dry THF (90 mL), followed by the addition of $NaHCO_3$ (2.0 g, 23.8 mmol, 2.4 equiv.). After 5 min, DMAP (50 mg, 0.40 mmol, 0.04 equiv.) and *p*-toluidine (1.67 g, 15.6 mmol, 1.6 equiv.) were added consecutively. The mixture was then stirred at rt for 24 h. THF was evaporated, the residue dissolved in CH_2Cl_2 (50 mL), and extracted first with HCl (1 M, 2 × 50 mL) and then with NaOH (1 M, 2 × 50 mL). The organic phase was dried with Na_2SO_4, filtered, and the solvent evaporated under reduced pressure to yield compound **4** (1.92 g, 81 % yield) as an off-white solid. Spectroscopic data were in accordance to those reported previously [48].

4.1.5.5. N-(p-tolyl)cinnamamide (4) [48]. R_f: 0.60 (EtOAc/*n*-hexanes 1/1); ^{1}H NMR (400 MHz, $CDCl_3$) δ 2.33 (s, 3 H, Ar-CH_3), 6.54 (d, J = 15.4, 1 H, C*H*), 7.13–7.18 (m, 2 H, Ar-*H*), 7.32 (br s, 1 H, CON*H*), 7.36–7.42 (m, 3 H, Ar-*H*), 7.46–7.60 (m, 4 H, Ar-*H*), 7.75 (d, J = 15.4 Hz, 1 H, C*H*); HRMS (ESI) *m/z* calcd for $C_{16}H_{16}NO$ $[M+H]^+$ 238.1226, found 238.1223.

To compound **4** (964 mg, 4.0 mmol, 1.0 equiv.), $AlCl_3$ (1.6 g, 12.0 mmol, 3.0 equiv.) was added and heated until it melted. The dark brown oil was then stirred at 100 °C for 1 h. After mixture achieved rt, cooled (0 °C) H_2O (20 mL) was added. The resulting precipitate was filtered off, dissolved in EtOAc (50 mL), and extracted with H_2O (50 mL). The aqueous phase was further washed with EtOAc (2 × 30 mL) and the combined organic phases were extracted with brine (100 mL), dried with Na_2SO_4, filtered, and evaporated under reduced pressure to give compound **5** (557 mg, 87 % yield) as a red solid. Spectroscopic data were in accordance to those reported previously [48].

4.1.5.6. 6-Methylquinolin-2(1H)-one (5) [48]. R_f: 0.14 (EtOAc/*n*-hexanes 1/1); ^{1}H NMR (400 MHz, $CDCl_3$) δ 2.42 (s, 3 H, Ar-CH_3), 6.69 (d, J = 9.5 Hz, 1 H, Ar-*H*), 7.29–7.37 (m, 3 H, Ar-*H*), 7.75 (d, J = 9.5 Hz, 1 H, Ar-*H*), 11.97 (br s, 1 H, N*H*); HRMS (ESI) *m/z* calcd for $C_{10}H_{10}NO$ $[M+H]^+$ 160.0757, found 160.0756.

Compound **5** (557 mg, 3.5 mmol, 1.0 equiv.) was dissolved in $POCl_3$ (5.2 mL, 8.6 g, 56 mmol, 16.0 equiv.) and the mixture stirred at reflux (110 °C) for 1 h. After cooling to rt, the reaction mixture was poured onto ice and the resulting suspension neutralized with NaOH. This was followed by washing with EtOAc (4 × 100 mL) and the combined

organic phases were extracted with brine (100 mL), dried with Na_2SO_4, filtered, and evaporated under reduced pressure to give the crude product. Compound **6** was purified by column chromatography using EtOAc/*n*-hexanes (1/13) as an eluent system. Spectroscopic data were identical to those reported previously [49].

4.1.5.7. 2-Chloro-6-methylquinoline (6) [49]. Off-white solid; yield, 75 % (446 mg); R_f: 0.71 (EtOAc/*n*-hexanes 1/1); ^{1}H NMR (400 MHz, $CDCl_3$) δ 2.54 (s, 3 H, Ar-C*H*$_3$), 7.35 (d, J = 8.7 Hz, 1 H, Ar-*H*), 7.55–7.59 (m, 2 H, Ar-*H*), 7.92 (app dd, J = 8.5, 1.4 Hz, 1 H, Ar-*H*), 8.02 (dd, J = 8.5, 0.8 Hz, 1 H, Ar-*H*); HRMS (ESI) *m/z* calcd for $C_{10}H_9NCl$ $[M+H]^+$ 178.0418, found 178.0416.

4.1.5.8. 6-(Bromomethyl)-2-chloroquinoline6-(Bromomethyl)−2-chloroquinoline (7) [50]. The reaction was carried out according to the General procedure for bromination, starting from compound **6** (216 mg, 1.21 mmol), NBS (222 mg, 1.25 mmol), and dibenzoyl peroxide (15 mg, 0.06 mmol) in benzene. The mixture was stirred at 80 °C for 1 h. Compound was purified by column chromatography EtOAc/*n*-hexanes (1/5) as an eluent system to give compound **7** (122 mg, 57 % yield) as a pale-red solid. Spectroscopic data were identical to those reported previously [50]. R_f: 0.28 (EtOAc/*n*-hexanes 1/5); ^{1}H NMR (400 MHz, $CDCl_3$) δ 4.65 (s, 2 H, C*H*$_2$), 7.41 (d, J = 8.6 Hz, 1 H, Ar-*H*), 7.76 (dd, J = 8.7, 2.0 Hz, 1 H, Ar-*H*), 7.82 (d, J = 2.0 Hz, 1 H, Ar-*H*), 8.01 (d, J = 8.6 Hz, 1 H, Ar-*H*), 8.08 (d, J = 8.7 Hz, 1 H, Ar-*H*); HRMS (ESI) *m/z* calcd for $C_{10}H_8NBrCl$ $[M+H]^+$ 255.9523, found 255.9519.

4.1.6. Synthesis of S-substituted thiourea derivatives

4.1.6.1. Benzo[b]thiophen-5-ylmethyl carbamimidothioate hydrobromide salt (8). This compound was prepared according to the General procedure for the synthesis of thiourea derivatives, starting from compound **1** (983 mg, 4.33 mmol) and thiourea (428 mg, 5.63 mmol) in MeCN. Off-white solid; yield, 60 % (789 mg); R_f: 0.0 (CH_2Cl_2/MeOH 9/1); ^{1}H NMR (400 MHz, DMSO-d_6) δ 4.61 (s, 2 H, SC*H*$_2$), 7.41 (dd, J_1 = 8.4 Hz, J_2 = 1.6 Hz, 1 H, Ar-*H*), 7.47 (dd, J_1 = 5.3 Hz, J_2 = 0.6 Hz, 1 H, Ar-*H*), 7.83 (d, J = 5.3, 1 H, Ar-*H*), 7.92 (d, J = 1.2 Hz, 1 H, Ar-*H*), 8.03 (d, J = 8.4, 1 H, Ar-*H*) 8.97 (br s, 2 H, N*H*$_2^+$), 9.18 (br s, 2 H, N*H*$_2$); ^{13}C NMR (101 MHz, DMSO-d_6) δ 34.94, 123.55, 124.44, 124.29, 125.66, 129.09, 131.59, 139.20, 140.13, 169.45; HRMS (ESI) *m/z* calcd for $C_{10}H_{11}N_2S_2$ $[M]^+$ 223.0358, found 223.0358.

4.1.6.2. Benzo[d]thiazol-6-ylmethyl carbamimidothioate hydrobromide salt (9). This compound was prepared according to the General procedure for the synthesis of thiourea derivatives, starting from compound **2** (581 mg, 2.56 mmol) and thiourea (253 mg, 3.33 mmol) in MeCN. Orange solid; yield, 64 % (493 mg); R_f: 0.10 (acetone/*n*-hexanes 1/5); ^{1}H NMR (400 MHz, CD_3OD) δ 4.66 (s, 2 H, SC*H*$_2$), 7.66 (dd, J_1 = 8.5 Hz, J_2 = 1.8 Hz, 1 H, Ar-*H*), 8.10 (d, J = 8.6 Hz, 1 H, Ar-*H*), 8.20 (d, J = 1.8 Hz, 1 H, Ar-*H*), 9.31 (s, 1 H, Ar-*H*); ^{13}C NMR (101 MHz, DMSO-d_6) δ 34.06, 121.75, 122.16, 126.48, 131.22, 133.41, 133.37, 151.76, 156.00, 169.60; HRMS (ESI) *m/z* calcd for $C_9H_{10}N_3S_2$ $[M]^+$ 224.0307, found 224.0311.

4.1.6.3. (1H-benzo[d]imidazol-2-yl)methyl carbamimidothioate hydrochloride salt (10). This compound was prepared according to the General procedure for the synthesis of thiourea derivatives, starting from 2-(chloromethyl)−1*H*-benzo[*d*]imidazole (1.01 g, 6.07 mmol) and thiourea (601 mg, 7.89 mmol) in MeCN. Light brown solid; yield, 77 % (1.13 g); R_f: 0.15 (CH_2Cl_2/MeOH 9/1); ^{1}H NMR (400 MHz, DMSO-d_6) δ 4.76 (s, 2 H, SC*H*$_2$), 7.24 (dt, J_1 = 7.2 Hz, J_2 = 3.5 Hz, 2 H, Ar-*H*), 7.58 (dt, J_1 = 7.2 Hz, J_2 = 3.5 Hz, 2 H, Ar-*H*), 9.34 (s, 2 H, N*H*$_2^+$), 10.39 (br s, 2 H, N*H*$_2$); ^{13}C NMR (101 MHz, DMSO-d_6) δ 28.07, 115.52, 123.10, 138.17, 150.16, 170.24; HRMS (ESI) *m/z* calcd for $C_9H_{11}N_4S$ $[M]^+$ 227.0695, found 227.0699.

4.1.6.4. Quinolin-2-ylmethyl carbamimidothioate hydrobromide salt (11). This compound was prepared according to the General procedure for the synthesis of thiourea derivatives, starting from compound **3** (305 mg, 1.37 mmol) and thiourea (136 mg, 1.79 mmol) in MeCN. Orange solid; yield, 64 % (262 mg); R_f: 0.0 (EtOAc/*n*-hexanes 1/2); ^{1}H NMR (400 MHz, DMSO-d_6) δ 4.81 (s, 2 H, SC*H*$_2$), 7.64 (d, J = 8.4 Hz, 1 H, Ar-*H*), 7.65 (ddd, J_1 = 8.6 Hz, J_2 = 6.8 Hz, J_3 = 1.1 Hz, 1 H, Ar-*H*), 7.82 (ddd, J_1 = 8.8 Hz, J_2 = 6.9 Hz, J_3 = 1.5 Hz, 1 H, Ar-*H*), 7.97–8,05 (m, 2 H, Ar-*H*), 8.47 (d, J = 8.3 Hz, 1 H, Ar-*H*), 9.33 (br s, 4 H, N*H*$_2$ and N*H*$_2^+$); ^{13}C NMR (101 MHz, DMSO-d_6) δ 36.47, 121.35, 126.99, 127.12, 128.03, 128.11, 130.47, 138.07, 146.49, 156.32, 170.16; HRMS (ESI) *m/z* calcd for $C_{11}H_{12}N_3S$ $[M]^+$ 218.0749, found 217.0746.

4.1.6.5. (2-Chloroquinolin-6-yl)methyl carbamimidothioate hydrobromide salt (12). This compound was prepared according to the General procedure for the synthesis of thiourea derivatives, starting from compound **7** (58 mg, 0.22 mmol) and thiourea (23 mg, 0.30 mmol) in MeCN. Off-white solid; yield, 84 % (122 mg); R_f: 0 (CH_2Cl_2/MeOH 5/1); ^{1}H NMR (400 MHz, DMSO-d_6) δ 4.70 (s, 2 H, SC*H*$_2$), 7.63 (d, J = 8.6 Hz, 1 H, Ar-*H*), 7.86 (dd, J = 8.7, 2.0 Hz, 1 H, Ar-*H*), 7.99 (d, J = 8.7 Hz, 1 H, Ar-*H*), 8.06 (d, J = 2.0 Hz, 1 H, Ar-*H*), 8.46 (d, J = 8.6 Hz, 1 H, Ar-*H*), 9.02 (br s, 2 H, N*H*$_2^+$), 9.25 (br s, 2 H, N*H*$_2$); ^{13}C NMR (101 MHz, DMSO-d_6) δ 34.42, 123.41, 126.93, 128.43, 128.93, 132.28, 134.95, 140.37, 147.06, 150.67, 169.47; HRMS (ESI) *m/z* calcd for $C_{11}H_{11}N_3ClS$ $[M]^+$ 252.0357, found 252.0353.

4.1.6.6. (5-Chlorobenzo[b]thiophen-3-yl)methyl carbamimidothioate hydrobromide salt (13a) and 3-(bromomethyl)− 5-chlorobenzo[b]thiophen-2-yl carbamimidothioate hydrobromide salt (13b). These compounds were prepared according to the General procedure for the synthesis of thiourea derivatives, starting from 3-(bromomethyl)− 5-chlorobenzo[*b*]thiophene (2.39 g, 9.12 mmol) and thiourea (903 mg, 11.86 mmol) in MeCN.

13a: R_f: 0 (CH_2Cl_2/MeOH 9/1); ^{1}H NMR (400 MHz, DMSO-d_6) δ 4.79 (s, 2 H, SC*H*$_2$), 7.46 (dd, J_1 = 8.6 Hz, J_2 = 2.0 Hz, 1 H, Ar-*H*), 7.92 (s, 1 H, Ar-*H*), 8.08 (d, J = 8.6 Hz, 1 H, Ar-*H*), 8.16 (d, J = 2.0 Hz, 1 H, Ar-*H*), 9.20 (br s, 4 H, N*H*$_2$ and N*H*$_2^+$); HRMS (ESI) *m/z* calcd for $C_{10}H_{10}ClN_2S_2^+$ $[M]^+$ 256.9968, found 256.9962.

13b: R_f: 0 (CH_2Cl_2/MeOH 9/1); ^{1}H NMR (400 MHz, DMSO-d_6) δ 4.79 (s, 2 H, C*H*$_2$), 7.51 (dd, J_1 = 8.6 Hz, J_2 = 2.0 Hz, 1 H, Ar-*H*), 8.07 (d, J = 8.6 Hz, 1 H, Ar-*H*), 8.19 (d, J = 2.0 Hz, 1 H, Ar-*H*), 9.20 (br s, 4 H, N*H*$_2$ and N*H*$_2^+$); HRMS (ESI) *m/z* calcd for $C_{10}H_9BrClN_2S_2^+$ $[M]^+$ 334.9074, found 334.9078.

4.1.6.7. 3-(Trifluoromethyl)benzyl carbamimidothioate hydrochloride salt (14). This compound was prepared according to the General procedure for the synthesis of thiourea derivatives, starting from 1-(chloromethyl)−3-(trifluoromethyl)benzene (582 mg, 3.0 mmol) and thiourea (297 mg, 3.9 mmol) in MeCN. White solid; yield, 55 % (318 mg); R_f: 0 (CH_2Cl_2/MeOH 5/1); ^{1}H NMR (400 MHz, DMSO-d_6) δ 4.64 (s, 2 H, SC*H*$_2$), 7.63 (t, J = 7.7 Hz, 1 H, Ar-*H*), 7.67–7.72 (m, 1 H, Ar-*H*), 7.70–7.74 (m, 1 H, Ar-*H*), 7.83–7.86 (m, 1 H, Ar-*H*), 9.32 (br s, 4 H, N*H*$_2$ and N*H*$_2^+$); ^{13}C NMR (101 MHz, DMSO-d_6) δ 33.67, 124.49 (q, $^1J_{F,C}$ = 272.4 Hz), 125.09 (q, $^3J_{F,C}$ = 3.8 Hz), 126.01 (q, $^3J_{F,C}$ = 3.7 Hz), 129.80 (q, $^2J_{F,C}$ = 31.7 Hz), 130.33, 133.56, 137.81, 169.19; HRMS (ESI) *m/z* calcd for $C_9H_{10}N_2F_3S$ $[M]^+$ 235.0511, found 235.0507.

4.1.6.8. (2-Methylthiazol-4-yl)methyl carbamimidothioate hydrochloride salt (15). This compound was prepared according to the General procedure for the synthesis of thiourea derivatives, starting from 4-(chloromethyl)− 2-methylthiazole hydrochloride salt (2.27 g, 12.4 mmol) and thiourea (1.23 g, 16.1 mmol) in MeCN. Prior to use in General procedure, the thiazole was dissolved in saturated aqueous solution of $NaHCO_3$ (50 mL), followed by washing of the aqueous phase with CH_2Cl_2 (4 × 40 mL). The combined organic phases were dried with

Na_2SO_4, filtered, and evaporated under reduced pressure to obtain a free form of compound. White solid; yield, 69 % (1.78 g); R_f: 0.0 (CH_2Cl_2/MeOH 1/9); ^{1}H NMR (400 MHz, DMSO-d_6) δ 2.65 (s, 3 H, CH_3), 4.57 (s, 2 H, SCH_2), 7.52 (s, 1 H, Ar-*H*), 9.41 (br s, 4 H, NH_2 and NH_2^+); ^{13}C NMR (101 MHz, DMSO-d_6) δ 19.18, 30.47, 118.29, 149.44, 167.33, 170.13; HRMS (ESI) *m/z* calcd for $C_6H_{10}N_3S_2$ $[M]^+$ 188.0310, found 188.0309.

4.1.7. Synthesis of 6-substituted 4-mercapto-1,3,5-triazin-2(1H)-ones

4.1.7.1. 6-((Benzo[b]thiophen-5-ylmethyl)thio)− 4-mercapto-1,3,5-triazin-2(1 H)-one (16). This compound was prepared according to the General procedure for the synthesis of 6-substituted 4-mercapto-1,3,5-triazin-2(1*H*)-ones, starting from compound **8** (789 mg, 2.6 mmol) and ethoxycarbonyl isothiocyanate (429 µl, 477 mg, 3.64 mmol). The mixture was stirred for 24 h. Compound was purified by column chromatography using CH_2Cl_2/MeOH (15/1) as an eluent system to give **16** (264 mg, 32 % yield) as a yellow solid. R_f: 0.26 (CH_2Cl_2/MeOH 9/1); ^{1}H NMR (400 MHz, DMSO-d_6) δ 4.50 (s, 2 H, SCH_2), 7.42 (dd, J_1 = 8.3 Hz, J_2 = 1.6 Hz, 1 H, Ar-*H*), 7.43 (dd, J_1 = 5.2 Hz, J_2 = 0.5 Hz, 1 H, Ar-*H*), 7.78 (d, J = 5.2 Hz, 1 H, Ar-*H*), 7.92 (d, J = 1.1 Hz, 1 H, Ar-*H*), 7.96 (d, J = 8.3 Hz, 1 H, Ar-*H*), 12.38 (br s, 1 H), 13.60 (br s, 1 H); ^{13}C NMR (101 MHz, DMSO-d_6) δ 34.20, 123.23, 124.29, 124.57, 125.99, 128.69, 132.96, 138.79, 140.09, 148.41, 150.39, 178.86 (br s); HRMS (ESI) *m/z* calcd for $C_{12}H_8N_3OS_3$ $[M–H]^-$ 305.9836, found 305.9835.

4.1.7.2. 6-((Benzo[d]thiazol-6-ylmethyl)thio)−4-mercapto-1,3,5-triazin-2(1H)-one (17). This compound was prepared according to the General procedure for the synthesis of 6-substituted 4-mercapto-1,3,5-triazin-2 (1*H*)-ones, starting from compound **9** (250 mg, 0.83 mmol) and ethoxycarbonyl isothiocyanate (137 µl, 131 mg, 1.16 mmol). The mixture was stirred for 24 h. Compound was purified by column chromatography using CH_2Cl_2/MeOH (30/1 to 5/1) as an eluent system to give **17** (22 mg, 9 % yield) as a yellow solid. R_f: 0.47 (CH_2Cl_2/MeOH 4/1); ^{1}H NMR (400 MHz, DMSO-d_6) δ 4.43 (s, 2 H, SCH$_2$), 7.58 (dd, J_1 = 8.4 Hz, J_2 = 1.7 Hz, 1 H, Ar-*H*), 8.02 (d, J = 8.4 Hz, 1 H, Ar-*H*), 8.18 (d, J = 1.7 Hz, 1 H, Ar-*H*), 9.36 (s, 1 H, Ar-*H*), 11.33 (br s, 1 H); ^{13}C NMR (101 MHz, DMSO-d_6) δ 33.37, 122.50, 122.84, 127.52, 133.65, 139.27, 152.15, 156.10, 161.99 (br s), 176.58 (br s); Purity by UHPLC: 99.4 %; HRMS (ESI) *m/z* calcd for $C_{11}H_9N_4OS_3$ $[M+H]^+$ 308.9933, found 308.9933.

4.1.7.3. 6-(((1H-benzo[d]imidazol-2-yl)methyl)thio)− 4-mercapto-1,3,5-triazin-2(1 H)-one (18). To a cooled (0 °C) suspension of compound **10** (301 mg, 1.24 mmol, 1.0 equiv.) in dry THF (15 mL), ethoxycarbonyl isothiocyanate (176 µl, 195 mg, 1.16 mmol, 1.2 equiv.) and KOtBu (419 mg, 3.73 mmol, 3.0 equiv.) were added under argon atmosphere. The reaction mixture was stirred at 70 °C for 24 h. After cooling to rt, the volatiles were evaporated under reduced pressure and the product was purified by column chromatography using CH_2Cl_2/MeOH (9/1 to 5/1) as an eluent system to give **18** (85 mg, 24 % yield) as a yellow solid. R_f: 0.24 (CH_2Cl_2/MeOH 4/1); ^{1}H NMR (400 MHz, DMSO-d_6) δ 4.45 (s, 2 H, SCH$_2$), 7.11–7.16 (m, 2 H, Ar-*H*), 7.44–7.51 (m, 2 H, Ar-*H*), 11.07 (br s, 1 H), 12.41 (br s, 1 H); HRMS (ESI) *m/z* calcd for $C_{11}H_{10}N_5OS_2$ $[M+H]^+$ 292.0245, found 292.0248.

4.1.7.4. 4-Mercapto-6-((quinolin-2-ylmethyl)thio)−1,3,5-triazin-2(1H)-one (19). This compound was prepared according to the General procedure for the synthesis of 6-substituted 4-mercapto-1,3,5-triazin-2(1*H*)-ones, starting from compound **11** (262 mg, 0.88 mmol) and ethoxycarbonyl isothiocyanate (145 µl, 162 mg, 1.23 mmol). The mixture was stirred for 24 h. Compound was purified by column chromatography using CH_2Cl_2/MeOH (15/1) as an eluent system to give **19** (20 mg, 8 % yield) as an off-white solid. R_f: 0.32 (CH_2Cl_2/MeOH 9/1); ^{1}H NMR (400 MHz, DMSO-d_6) δ 4.71 (s, 2 H, SCH_2), 7.61 (ddd, J_1 = 8.4 Hz, J_2 = 7.0 Hz, J_3 = 1.1 Hz, 1 H, Ar-*H*), 7.67 (d, J = 8.4 Hz, 1 H, Ar-*H*), 7.78 (ddd, J_1 = 8.7 Hz, J_2 = 6.8 Hz, J_3 = 1.2 Hz, 1 H, Ar-*H*) 7.96–8.02 (m, 2 H, Ar-*H*), 8.37 (d, J = 8.6 Hz, 1 H, Ar-*H*), 12.52 (br s, 1 H), 13.83 (br s, 1 H); ^{13}C NMR (101 MHz, DMSO-d_6) δ 31.13, 121.23, 128.50, 129.19, 129.33, 129.76, 131.31, 138.65, 148.43, 150.41, 150.91 (br s), 166.59, 178.91 (br s); HRMS (ESI) *m/z* calcd for $C_{13}H_{11}N_4OS_2$ $[M+H]^+$ 303.3702, found 303.3701.

4.1.7.5. 6-(((2-Chloroquinolin-6-yl)methyl)thio)−4-mercapto-1,3,5-triazin-2(1H)-one (20). This compound was prepared according to the General procedure for the synthesis of 6-substituted 4-mercapto-1,3,5-triazin-2(1*H*)-ones, starting from compound **12** (122 mg, 0.42 mmol) and ethoxycarbonyl isothiocyanate (70 µl, 78 mg, 0.60 mmol). The mixture was stirred for 24 h. Compound was purified by column chromatography using CH_2Cl_2/MeOH (9/1) as an eluent system to give **20** (75 mg, 52 % yield) as a yellow solid. R_f: 0.16 (CH_2Cl_2/MeOH, 9/1); ^{1}H NMR (400 MHz, DMSO-d_6) δ 4.50 (s, 2 H, SCH_2), 7.58 (d, J = 8.7 Hz, 1 H, Ar-*H*), 7.86 (dd, J = 8.7, 2.0 Hz, 1 H, Ar-*H*), 7.91 (d, J = 8.7 Hz, 1 H, Ar-*H*), 8.05 (d, J = 2.0 Hz, 1 H, Ar-*H*), 8.40 (d, J = 8.7 Hz, 1 H, Ar-*H*), 11.72 (br s, 1 H, N*H*), 13.66 (br s, 1 H); ^{13}C NMR (101 MHz, DMSO-d_6) δ 33.24, 122.21, 126.30, 126.50, 128.15, 128.25, 134.47, 137.06, 146.56, 147.99, 150.13 (br s), 167.91, 178.42 (br s); HRMS (ESI) *m/z* calcd for $C_{13}H_{10}N_4OClS_2$ $[M+H]^+$ 336.9979, found 336.9974.

4.1.7.6. 6-(((5-Chlorobenzo[b]thiophen-3-yl)methyl)thio)−4-mercapto-1,3,5-triazin-2(1H)-one (21a) and 6-((3-(bromomethyl)−5-chlorobenzo [b]thiophen-2-yl)thio)−4-mercapto-1,3,5-triazin-2(1H)-one (21b). These compounds were prepared according to the General procedure for the synthesis of 6-substituted 4-mercapto-1,3,5-triazin-2(1*H*)-ones, starting from compound a mixture of compounds **13a** and **13b** (1.4 g, 4.1 mmol [calc. for Mw of **13a**]) and ethoxycarbonyl isothiocyanate (677 µl, 755 mg, 5.75 mmol). The mixture was stirred for 24 h. After washing the resulting solid with *n*-hexanes and drying, 329 mg of an off-white solid was obtained. The ^{1}H NMR analysis revealed that the **21a**/**21b** molar ratio was 0.26 (it remained the same during the cyclization step).

21a: R_f: 0.16 (CH_2Cl_2/MeOH 9/1); ^{1}H NMR (400 MHz, DMSO-d_6) δ 4.60 (s, 2 H, SCH_2), 7.43 (dd, J_1 = 8.6 Hz, J_2 = 2.1 Hz, 1 H, Ar-*H*), 7.87 (s, 1 H, Ar-*H*), 8.05 (d, J = 8.6 Hz, 1 H, Ar-*H*), 8.06 (d, J = 2.0 Hz, 1 H, Ar-*H*), 11.93 (br s, 1 H), 13.61 (br s, 1 H); HRMS (ESI) *m/z* calcd for $C_{12}H_7ClN_3OS_3$ $[M–H]^-$ 339.9445, found 339.9446.

21b: R_f: 0.16 (CH_2Cl_2/MeOH 9/1); ^{1}H NMR (400 MHz, DMSO-d_6) δ 4.61 (s, 2 H, CH_2), 7.46 (dd, J_1 = 8.6 Hz, J_2 = 2.1 Hz, 1 H, Ar-*H*), 8.03 (d, J = 8.6 Hz, 1 H, Ar-*H*), 8.09 (d, J = 2.0 Hz, 1 H, Ar-*H*), 12.04 (br s, 1 H), 13.60 (br s, 1 H); HRMS (ESI) *m/z* calcd for $C_{12}H_6ClN_3OBrS_3$ $[M–H]^-$ 417.8550, found 417.8554.

4.1.7.7. 4-Mercapto-6-((3-(trifluoromethyl)benzyl)thio)−1,3,5-triazin-2 (1H)-one (22). This compound was prepared according to the General procedure for the synthesis of 6-substituted 4-mercapto-1,3,5-triazin-2 (1*H*)-ones, starting from compound **14** (194 mg, 1.0 mmol) and ethoxycarbonyl isothiocyanate (165 µl, 184 mg, 1.4 mmol). The mixture was stirred for 24 h. Compound **22** was sufficiently pure after washing of the precipitate with *n*-hexanes. Yellow solid; yield, 41 % (130 mg); R_f: 0.11 (EtOAc/*n*-hexanes 1/1); ^{1}H NMR (400 MHz, DMSO-d_6) δ 4.46 (s, 2 H, SCH_2), 7.57 (t, J = 7.8 Hz, 1 H, Ar-*H*), 7.62–7.67 (m, 1 H, Ar-*H*), 7.73–7.78 (m, 1 H, Ar-*H*), 7.81–7.85 (m, 1 H, Ar-*H*), 12.54 (br s, 1 H), 13.68 (br s, 1 H); ^{13}C NMR (101 MHz, DMSO-d_6) δ 33.24, 124.56 (q, $^1J_{F,C}$ = 272.2 Hz, *C*F$_3$), 124.68 (q, $^3J_{F,C}$ = 4.0 Hz), 126.33 q, $^3J_{F,C}$ = 3.9 Hz), 129.60 (q, $^2J_{F,C}$ = 31.5 Hz), 130.04, 133.87, 138.82, 150.35 (br s), 168.29, 178.14 (br s); HRMS (ESI) *m/z* calcd for $C_{11}H_9N_3OF_3S_2$ $[M+H]^+$ 320.0134, found 320.0131.

4.1.7.8. 4-Mercapto-6-(((2-methylthiazol-4-yl)methyl)thio)−1,3,5-triazin-2(1H)-one (23). This compound was prepared according to the General procedure for the synthesis of 6-substituted 4-mercapto-1,3,5-triazin-2(1*H*)-ones, starting from compound **15** (1.78 g, 8.0 mmol) and

ethoxycarbonyl isothiocyanate (1.32 mL, 1.47 g, 11.2 mmol). The mixture was stirred for 24 h. Compound **23** was sufficiently pure after washing of the precipitate with *n*-hexanes. Off-white solid; yield, 21 % (448 mg); R_f: 0.10 (CH_2Cl_2/MeOH 9/1); ^{1}H NMR (400 MHz, DMSO-d_6) δ 2.63 (s, 3 H, CH_3), 4.42 (s, 2 H, SCH_2), 7.43 (s, 1 H, Ar-*H*), 12.49 (br s, 1 H), 13.63 (br s, 1 H); ^{13}C NMR (101 MHz, DMSO-d_6) δ 18.72, 29.56, 117.23, 145.98, 149.57, 150.18 (br s), 166.85, 168.95, 178.40 (br s); Purity by LC-MS: 98.9 %; HRMS (ESI) *m/z* calcd for $C_8H_8ON_4S_3$ $[M+H]^+$ 272.9933, found 272.9932.

4.1.8. Synthesis of 4,6-disubstituted-1,3,5-triazin-2(1H)-ones

4.1.8.1. 6-((Benzo[b]thiophen-5-ylmethyl)thio)−4-((3-fluoro-5-(trifluoromethyl)benzyl)thio)−1,3,5-triazin-2(1H)-one (24). This compound was prepared according to the General procedure for the synthesis of 4,6-disubstituted 1,3,5-triazin-2(1*H*)-ones, starting from compound **16** (264 mg, 0.86 mmol) and 1-(bromomethyl)−3-fluoro-5-(trifluoromethyl)benzene (243 mg, 0.95 mmol). Compound **24** was sufficiently pure after precipitate formation. White solid; yield, 78 % (324 mg); R_f: 0.70 (CH_2Cl_2/MeOH, 9/1); ^{1}H NMR (400 MHz, DMSO-d_6) δ 4.45 (s, 2 H, SCH_2), 4.49 (s, 2 H, SCH_2), 7.38 (dd, J_1 = 8.3 Hz, J_2 = 1.6 Hz, 1 H, Ar-*H*), 7.41 (dd, J_1 = 5.5 Hz, J_2 = 0.5 Hz, 1 H, Ar-*H*), 7.54–7.63 (m, 2 H, Ar-*H*), 7.68 (s, 1 H, Ar-*H*), 7.77 (d, J = 5.4 Hz, 1 H, Ar-*H*), 7.89 (d, J = 1.2 Hz, 1 H, Ar-*H*), 7.95 (d, J = 8.3 Hz, 1 H, Ar-*H*), 13.05 (bs, 1 H, N*H*); ^{13}C NMR (101 MHz, DMSO-d_6) δ 33.05, 34.25, 112.17 (dq, $^2J_{F,C}$ = 25.2 Hz, $^3J_{F,C}$ = 3.4 Hz), 120.65 (d, $^2J_{F,C}$ = 21.9 Hz), 122.53 (q, $^3J_{F,C}$ = 3.7 Hz), 123.17, 123.69 (dd, $^1J_{F,C}$ = 270.4 Hz, $^4J_{F,C}$ = 3.1 Hz), 124.22, 124.39, 125.84, 128.65, 131.32 (qd, $^2J_{F,C}$ = 32.5 Hz, $^3J_{F,C}$ = 8.4 Hz), 133.15, 138.69, 140.06, 142.67 (d, $^3J_{F,C}$ = 8.1 Hz), 150.40, 162.23 (d, $^1J_{F,C}$ = 246.7 Hz), 176.42 (br s); Purity by UHPLC: 97.3 %; HRMS (ESI) *m/z* calcd for $C_{20}H_{12}N_3OF_4S_3$ $[M-H]^-$ 482.0084, found 482.0085.

4.1.8.2. 6-((Benzo[b]thiophen-5-ylmethyl)thio)−4-((4-(trifluoromethyl)benzyl)thio)−1,3,5-triazin-2(1H)-one (25). This compound was prepared according to the General procedure for the synthesis of 4,6-disubstituted 1,3,5-triazin-2(1*H*)-ones, starting from compound **16** (264 mg, 0.86 mmol) and 1-(bromomethyl)−4-(trifluoromethyl)benzene (227 mg, 0.95 mmol). Compound **25** was sufficiently pure after precipitate formation. White solid; yield, 76 % (304 mg); R_f: 0.68 (CH_2Cl_2/MeOH, 9/1); ^{1}H NMR (400 MHz, DMSO-d_6) δ 4.43 (s, 2 H, SCH_2), 4.47 (s, 2 H, SCH_2), 7.38 (dd, J_1 = 8.3 Hz, J_2 = 1.6 Hz, 1 H, Ar-*H*), 7.41 (dd, J_1 = 5.4 Hz, J_2 = 0.5 Hz, 1 H, Ar-*H*), 7.58–7.62 (m, 2 H, Ar-*H*), 7.63–7.68 (m, 2 H, Ar-*H*), 7.77 (d, J = 5.4 Hz, 1 H, Ar-*H*), 7.88 (d, J = 1.1 Hz, 1 H, Ar-*H*), 7.94 (d, J = 8.3 Hz, 1 H, Ar-*H*), 12.97 (br s, 1 H, N*H*); ^{13}C NMR (101 MHz, DMSO-d_6) δ 33.38, 34.19, 123.18, 124.25, 124.35, 125.76 (q, $^3J_{F,C}$ = 3.9 Hz), 125.85, 127.02 (q, $^1J_{F,C}$ = 272.3 Hz), 128.30 (d, $^2J_{F,C}$ = 31.9 Hz), 128.64, 130.19, 133.28, 138.67, 140.08, 142.74, 150.40, 154.37 (br s), 175.74 (br s); Purity by LC-MS: 95.3 %; HRMS (ESI) *m/z* calcd for $C_{20}H_{13}N_3OF_3S_3$ $[M+H]^+$ 464.0178, found 464.0178.

4.1.8.3. 6-((Benzo[b]thiophen-5-ylmethyl)thio)−4-((4-isopropylbenzyl)thio)−1,3,5-triazin-2(1H)-one (26). This compound was prepared according to the General procedure for the synthesis of 4,6-disubstituted 1,3,5-triazin-2(1*H*)-ones, starting from compound **16** (264 mg, 0.86 mmol) and 1-(bromomethyl)−4-isopropylbenzene (202 mg, 0.95 mmol). Compound **26** was sufficiently pure after precipitate formation. White solid; yield, 55 % (208 mg); R_f: 0.62 (CH_2Cl_2/MeOH, 9/1); ^{1}H NMR (400 MHz, DMSO-d_6) δ 1.16 (d, J = 6.9 Hz, 6 H, Ar-CH(CH_3)$_2$), 2.84 (sept, J = 6.9 Hz, 1 H, Ar-C*H*(CH$_3$)$_2$), 4.33 (s, 2 H, SCH_2), 4.51 (s, 2 H, SCH_2), 7.14–7.19 (m, 2 H, Ar-*H*), 7.27–7.31 (m, 2 H, Ar-*H*), 7.40 (dd, J_1 = 8.3 Hz, J_2 = 1.5 Hz, 1 H, Ar-*H*), 7.42 (dd, J_1 = 5.5 Hz, J_2 = 0.6 Hz, 1 H, Ar-*H*), 7.78 (d, J = 5.5 Hz, 1 H, Ar-*H*), 7.90 (d, J = 1.2 Hz, 1 H, Ar-*H*), 7.95 (d, J = 8.4 Hz, 1 H, Ar-*H*), 12.99 (br s, 1 H, N*H*); ^{13}C NMR (101 MHz, DMSO-d_6) δ 24.28, 33.57, 33.91, 34.26, 123.21, 124.29, 124.37, 125.88, 126.94, 128.66, 129.46, 133.33, 134.38, 138.69, 140.11, 148.11, 150.41, 165.71 (br s), 176.74 (br s); Purity by LC-MS: 95.8 %; HRMS (ESI) *m/z* calcd for $C_{22}H_{22}N_3OS_3$ $[M+H]^+$ 440.0920, found 440.0918.

4.1.8.4. 6-((Benzo[d]thiazol-6-ylmethyl)thio)−4-((3-fluoro-5-(trifluoromethyl)benzyl)thio)−1,3,5-triazin-2(1H)-one (27). This compound was prepared according to the General procedure for the synthesis of 4,6-disubstituted 1,3,5-triazin-2(1*H*)-ones, starting from compound **17** (20 mg, 0.06 mmol) and 1-(bromomethyl)−3-fluoro-5-(trifluoromethyl)benzene (18 mg, 0.07 mmol). Compound **27** was sufficiently pure after precipitate formation. Off-white solid; yield, 38 % (11 mg); R_f: 0.35 (CH_2Cl_2/MeOH 9/1); ^{1}H NMR (400 MHz, DMSO-d_6) δ 4.45 (s, 2 H, SCH_2), 4.52 (s, 2 H, SCH_2), 7.53–7.62 (m, 3 H, Ar-*H*), 7.67–7.69 (m, 1 H, Ar-*H*), 8.02 (d, J = 8.4 Hz, 1 H, Ar-*H*), 8.17 (d, J = 1.3 Hz, 1 H, Ar-*H*), 9.37 (s, 1 H, Ar-*H*), 11.17 (br s, 1 H, N*H*); ^{13}C NMR (101 MHz, DMSO-d_6) δ 32.57, 33.54, 111.90 (dq, $^2J_{F,C}$ = 24.4 Hz, $^3J_{F,C}$ = 3.4 Hz), 120.22 (d, $^2J_{F,C}$ = 21.4 Hz), 122.09 (q, $^3J_{F,C}$ = 3.7 Hz), 122.71, 122.95, 123.20 (dd, $^1J_{F,C}$ = 272.8 Hz, $^4J_{F,C}$ = 3.1 Hz), 127.44, 131.03 (qd, $^2J_{F,C}$ = 32.5 Hz, $^3J_{F,C}$ = 8.6 Hz), 133.76, 134.36 (br s), 142.17 (d, $^3J_{F,C}$ = 7.8 Hz), 149.95 (br s), 152.35, 156.46, 156.79 (br s), 161.79 (d, $^1J_{F,C}$ = 246.5 Hz), 172.30 (br s); Purity by UHPLC: 100.0 %; HRMS (ESI) *m/z* calcd for $C_{19}H_{12}ON_4F_4S_3$ $[M+H]^+$ 485.0182, found 485.0185.

4.1.8.5. 6-(((1 H-benzo[d]imidazol-2-yl)methyl)thio)−4-((3-fluoro-5-(trifluoromethyl)benzyl)thio)−1,3,5-triazin-2(1H)-one (28). This compound was prepared according to the General procedure for the synthesis of 4,6-disubstituted 1,3,5-triazin-2(1*H*)-ones, starting from compound **18** (53 mg, 0.18 mmol) and 1-(bromomethyl)−3-fluoro-5-(trifluoromethyl)benzene (51 mg, 0.20 mmol). Compound was purified additionally by column chromatography using CH_2Cl_2/MeOH (9/1) as an eluent system to give **28** (23 mg, 27 % yield) as a yellow solid. R_f: 0.32 (CH_2Cl_2/MeOH 9/1); ^{1}H NMR (400 MHz, DMSO-d_6) δ 4.41 (s, 2 H, SCH_2), 4.54 (s, 2 H, SCH_2), 7.12–7.17 (m, 2 H, Ar-*H*), 7.45–7.50 (m, 2 H, Ar-*H*), 7.52–7.56 (m, 1 H, Ar-*H*), 7.60 (app d, J = 9.2 Hz, 1 H, Ar-*H*), 7.65–7.69 (m, 1 H, Ar-*H*); ^{13}C NMR (101 MHz, DMSO-d_6) δ 27.23, 32.23, 111.58 (dq, $^2J_{F,C}$ = 24.7 Hz, $^3J_{F,C}$ = 3.8 Hz), 114.90 (br s), 120.14 (d, $^2J_{F,C}$ = 21.9 Hz), 121.79, 122.01 (q, $^3J_{F,C}$ = 3.7 Hz), 123.04 (dd, $^1J_{F,C}$ = 272.3 Hz, $^4J_{F,C}$ = 3.3 Hz), 123.39 (br s), 130.84 (qd, $^2J_{F,C}$ = 32.5 Hz, $^3J_{F,C}$ = 8.6 Hz), 138.74 (br s), 142.92 (d, $^3J_{F,C}$ = 7.8 Hz), 150.41, 157.03 (br s), 161.78 (d, $^1J_{F,C}$ = 246.0 Hz), 175.94 (br s); Purity by UHPLC: 95.2 %; HRMS (ESI) *m/z* calcd for $C_{19}H_{13}ON_5F_4S_2$ $[M+H]^+$ 468.0570, found 468.0571.

4.1.8.6. 4-((3-Fluoro-5-(trifluoromethyl)benzyl)thio)−6-((quinolin-2-ylmethyl)thio)−1,3,5-triazin-2(1H)-one (29). This compound was prepared according to the General procedure for the synthesis of 4,6-disubstituted 1,3,5-triazin-2(1*H*)-ones, starting from compound **19** (21 mg, 0.07 mmol) and 1-(bromomethyl)−3-fluoro-5-(trifluoromethyl)benzene (21 mg, 0.08 mmol). Compound **29** was sufficiently pure after precipitate formation. Off-white solid; yield, 18 % (6 mg); R_f: 0.58 (CH_2Cl_2/MeOH, 9/1); ^{1}H NMR (400 MHz, DMSO-d_6) δ 4.44 (s, 2 H, SCH_2), 4.65 (s, 2 H, SCH_2), 7.52–7.61 (m, 3 H, Ar-*H*), 7.62 (d, J = 8.4 Hz, 1 H, Ar-*H*), 7.65–7.68 (m, 1 H, Ar-*H*), 7.75 (ddd, J_1 = 8.4 Hz, J_2 = 7.0 Hz, J_3 = 1.5 Hz, 1 H, Ar-*H*) 7.91–7.98 (m, 2 H, Ar-*H*), 8.33 (d, J = 8.4 Hz, 1 H, Ar-*H*), 13.09 (br s, 1 H, N*H*); Purity by UHPLC: 95.1 %; HRMS (ESI) *m/z* calcd for $C_{21}H_{15}N_4OF_4S_2$ $[M+H]^+$ 479.0618, found 479.0615.

4.1.8.7. 6-(((2-Chloroquinolin-6-yl)methyl)thio)−4-((3-fluoro-5-(trifluoromethyl)benzyl)thio)−1,3,5-triazin-2(1H)-one (30). This compound was prepared according to the General procedure for the synthesis of 4,6-disubstituted 1,3,5-triazin-2(1*H*)-ones, starting from compound **20** (397 mg, 1.18 mmol) and 1-(bromomethyl)− 3-fluoro-5-(trifluoromethyl)benzene (334 mg, 1.30 mmol). Compound was purified

additionally by column chromatography using CH_2Cl_2/MeOH (9/1) as an eluent system to give **30** (230 mg, 38 % yield) as an off-white solid. *Note: the reaction was performed twice before the next step.* R_f: 0.49 (CH_2Cl_2/MeOH 9/1); ^{1}H NMR (400 MHz, $CDCl_3$) δ 4.37 (s, 2 H, SC*H*$_2$), 4.53 (s, 2 H, SC*H*$_2$), 7.18–7.25 (m, 1 H, Ar-*H*), 7.25–7.32 (m, 1 H, Ar-*H*), 7.37 (d, J = 8.7 Hz, 1 H, Ar-*H*), 7.40–7.46 (m, 1 H, Ar-*H*), 7.69 (d, J = 7.6 Hz, 1 H, Ar-*H*), 7.76–7.85 (m, 1 H, Ar-*H*), 7.96 (d, J = 8.6 Hz, 1 H, Ar-*H*), 8.03 (d, J = 7.6 Hz, 1 H, Ar-*H*), 12.64 (br s, 1 H, N*H*); ^{13}C NMR (101 MHz, DMSO-d_6) δ 32.29, 33.08, 111.50 (dq, $^2J_{F,C}$ = 24.2 Hz, $^3J_{F,C}$ = 3.7 Hz), 120.00 (d, $^2J_{F,C}$ = 22.0 Hz), 121.88 (q, $^3J_{F,C}$ = 3.7 Hz), 122.56, 123.10 (dd, $^1J_{F,C}$ = 272.9 Hz, $^4J_{F,C}$ = 3.7 Hz), 126.36, 127.55, 127.95, 130.69 (qd, $^2J_{F,C}$ = 32.3 Hz, $^3J_{F,C}$ = 8.8 Hz), 131.92, 136.34, 139.61, 142.41 (d, $^3J_{F,C}$ = 8.1 Hz), 146.34, 149.69, 155.07 (br s), 161.55 (d, $^1J_{F,C}$ = 246.5 Hz), 175.39 (br s); Purity by UHPLC: 95.2 %; HRMS (ESI) *m/z* calcd for $C_{21}H_{14}N_4OClF_4S_2$ $[M+H]^+$ 513.0228, found 513.0225.

4.1.8.8. 4-((3-Fluoro-5-(trifluoromethyl)benzyl)thio)−6-(((2-(2-morpholinoethoxy)quinolin-6-yl)methyl)thio)−1,3,5-triazin-2(1H)-one (31). To a cooled (0 °C) solution of 2-morpholinoethan-1-ol (216 mg, 1.66 mmol, 2.0 equiv.) in dry DMF (15 mL), NaH (60 %, 424 mg, 1.83 mmol, 1.1 equiv.) was added. After 30 min, a solution of **30** (424 mg, 0.83 mmol, 1.0 equiv.) in dry DMF (5 mL) was added dropwise at 0 °C. The reaction mixture was stirred at rt for 24 h, followed by the addition of H_2O (100 mL) to the mixture, which was subsequently extracted with EtOAc (3 × 30 mL). The combined organic phases were dried with Na_2SO_4, filtered, and the solvent evaporated to give the crude product. Compound **31** was purified by column chromatography using CH_2Cl_2/MeOH (15/1) as an eluent system. Off-white solid; yield, 5 % (26 mg); R_f: 0.41 (CH_2Cl_2/MeOH 9/1); ^{1}H NMR (400 MHz, DMSO-d_6) δ 2.51–2.60 (m, 4 H, morpholine-C*H*$_2$), 2.76 (t, J = 5.9 Hz, 2 H, NC*H*$_2$), 3.57 (t, J = 4.8 Hz, 4 H, morpholine-C*H*$_2$), 4.38 (s, 2 H, SC*H*$_2$), 4.45 (s, 2 H, SC*H*$_2$), 4.52 (t, J = 5.9 Hz, 2 H, C*H*$_2$O), 6.98 (d, J = 8.8 Hz, 1 H, Ar-*H*), 7.51–7.60 (m, 2 H, Ar-*H*), 7.62–7.70 (m, 3 H, Ar-*H*), 7.84 (d, J = 1.5 Hz, 1 H, Ar-*H*), 8.14 (d, J = 8.8 Hz, 1 H, Ar-*H*), 12.78 (br s, 1 H, N*H*); ^{13}C NMR (100 MHz, $CDCl_3$) δ 33.62, 34.54, 53.59, 57.24, 62.21, 66.23, 111.86 (dq, $^2J_{F,C}$ = 24.2 Hz, $^3J_{F,C}$ = 3.4 Hz), 113.40, 119.47 (d, $^2J_{F,C}$ = 20.5 Hz), 121.59 (app q, $^3J_{F,C}$ = 3.4 Hz), 124.84, 126.10 (dd, $^1J_{F,C}$ = 272.9 Hz, $^4J_{F,C}$ = 3.1 Hz), 127.51, 127.64, 130.45, 132.46 (d, $^2J_{F,C}$ = 32.3), 131.68, 138.46, 140.81 (d, $^3J_{F,C}$ = 7.1 Hz), 145.73, 159.37 (br s), 161.70, 162.35 (d, $^1J_{F,C}$ = 248.7 Hz), 177.73 (br s); Purity by LC-MS: 95.3 %; HRMS (ESI) *m/z* calcd for $C_{27}H_{26}N_5O_3F_4S_2$ $[M+H]^+$ 608.1408, found 608.1395.

4.1.8.9. 6-(((5-Chlorobenzo[b]thiophen-3-yl)methyl)thio)−4-((3-fluoro-5-(trifluoromethyl)benzyl)thio)−1,3,5-triazin-2(1H)-one (32). This compound was prepared according to the General procedure for the synthesis of 4,6-disubstituted 1,3,5-triazin-2(1*H*)-ones, starting from compound a mixture of compounds **21a** and **21b** (150 mg, 0.44 mmol [calc. for Mw of **21a**]) and 1-(bromomethyl)−3-fluoro-5-(trifluoromethyl)benzene (124 mg, 0.48 mmol). Compound was separated from **32b** and purified by column chromatography using EtOAc/*n*-hexanes/CH_3COOH (1/2/0.01) as an eluent system to give **32a** (11 mg, 4 % yield) as a white solid. R_f: 0.10 (EtOAc/*n*-hexanes/CH_3COOH 1/2/0.01); ^{1}H NMR (400 MHz, $CDCl_3$) δ 4.40 (s, 2 H, SC*H*$_2$), 4.61 (s, 2 H, SC*H*$_2$), 7.24 (app d, J = 8.4 Hz, 1 H, Ar-*H*), 7.28–7.31 (m, 1 H, Ar-*H*), 7.34 (dd, J_1 = 8.7 Hz, J_2 = 1.8 Hz, 1 H, Ar-*H*), 7.42–7.47 (m, 1 H, Ar-*H*), 7.56 (s, 1 H, Ar-*H*), 7.76 (d, J = 4.2 Hz, 1 H, Ar-*H*), 7.77 (d, J = 2.2 Hz, 1 H, Ar-*H*), 12.37 (br s, 1 H, N*H*); ^{13}C NMR (101 MHz, $CDCl_3$) δ 28.19, 34.08, 112.48 (dq, $^2J_{F,C}$ = 24.1 Hz, $^3J_{F,C}$ = 3.9 Hz), 119.87 (d, $^2J_{F,C}$ = 22.0 Hz), 121.49, 121.97 (q, $^3J_{F,C}$ = 3.3 Hz), 123.08 (dd, $^1J_{F,C}$ = 272.9 Hz, $^4J_{F,C}$ = 3.3 Hz), 124.17, 125.43, 128.40, 128.41, 128.89, 131.11, 138.61, 139.01, 140.07 (d, $^3J_{F,C}$ = 8.0 Hz), 155.48, 162.57 (d, $^1J_{F,C}$ = 250.0 Hz), 175.32 (br s); Purity by LC-MS: 95.1 %; HRMS (ESI) *m/z* calcd for $C_{20}H_{11}N_3OClF_4S_3$ $[M-H]^-$ 515.9694, found 515.9695.

4.1.8.10. 6-((3-(Bromomethyl)−5-chlorobenzo[b]thiophen-2-yl)thio)− 4-((3-fluoro-5-(trifluoromethyl)benzyl)thio)−1,3,5-triazin-2(1H)-one (32b). This compound was prepared according to the General procedure for the synthesis of 4,6-disubstituted 1,3,5-triazin-2(1*H*)-ones, starting from compound a mixture of compounds **21a** and **21b** (150 mg, 0.44 mmol [calc. for Mw of **21a**]) and 1-(bromomethyl)−3-fluoro-5-(trifluoromethyl)benzene (124 mg, 0.48 mmol). Compound was separated from **32** and purified by column chromatography using EtOAc/*n*-hexanes/CH_3COOH (1/2/0.01) as an eluent system to give **32b** (29 mg, 11 % yield) as a white solid. *Note: this compound was not evaluated in biochemical assays due to the high reactivity of the bromomethyl moiety.* R_f: 0.15 (EtOAc/*n*-hexanes/CH_3COOH 1/2/0.01); ^{1}H NMR (400 MHz, $CDCl_3$) δ 4.42 (s, 2 H, C*H*$_2$), 4.65 (s, 2 H, C*H*$_2$), 7.24 (app d, J = 8.3 Hz, 1 H, Ar-*H*), 7.30–7.36 (m, 2 H, Ar-*H*), 7.40–7.47 (m, 1 H, Ar-*H*), 7.64 (d, J = 8.6 Hz, 1 H, Ar-*H*), 7.84 (d, J = 2.0 Hz, 1 H, Ar-*H*), 11.94 (br s, 1 H, N*H*); ^{1}H NMR (400 MHz, DMSO-d_6) δ 4.47 (s, 2 H, C*H*$_2$), 4.62 (s, 2 H, C*H*$_2$), 7.46 (dd, J_1 = 8.6 Hz, J_2 = 2.1 Hz, 1 H, Ar-*H*), 7.57 (app d, J = 8.7 Hz, 1 H, Ar-*H*), 7.63 (app d, J = 9.5 Hz, 1 H, Ar-*H*), 7.66–7.70 (m, 1 H, Ar-*H*), 7.98–8.06 (m, 2 H, Ar-*H*), 13.13 (br s, 1 H, N*H*); ^{13}C NMR (101 MHz, DMSO-d_6) δ 26.48, 32.62, 112.48 (dq, $^2J_{F,C}$ = 24.5 Hz, $^3J_{F,C}$ = 3.0 Hz), 118.74, 120.23 (d, $^2J_{F,C}$ = 22.0 Hz), 121.76, 122.13 (q, $^3J_{F,C}$ = 3.4 Hz), 123.08 (dd, $^1J_{F,C}$ = 272.3 Hz, $^4J_{F,C}$ = 3.3 Hz), 124.22, 125.37, 129.56, 130.49, 130.84 (dd, $^2J_{F,C}$ = 32.8 Hz, $^3J_{F,C}$ = 8.6 Hz), 137.40, 138.30, 142.23 (d, $^3J_{F,C}$ = 8.0 Hz), 153.30 (br s), 161.78 (d, $^1J_{F,C}$ = 246.5 Hz), 174.44 (br s); Purity by UHPLC: 98.2 %; HRMS (ESI) *m/z* calcd for $C_{20}H_{12}N_3OClBrF_4S_3$ $[M+H]^+$ 595.8945, found 595.8942.

4.1.8.11. 6-(((5-Chlorobenzo[b]thiophen-3-yl)methyl)thio)−4-((4-(trifluoromethyl)benzyl)thio)−1,3,5-triazin-2(1H)-one (33). This compound was prepared according to the General procedure for the synthesis of 4,6-disubstituted 1,3,5-triazin-2(1*H*)-ones, starting from compound a mixture of compounds **21a** and **21b** (96 mg, 0.28 mmol [calc. for Mw of **21a**]) and 1-(bromomethyl)−4-(trifluoromethyl)benzene (74 mg, 0.31 mmol). Compound was separated from **33b** and purified by column chromatography using EtOAc/*n*-hexanes/CH_3COOH (1/2/0.01) as an eluent system to give **33** (7 mg, 5 % yield) as a white solid. R_f: 0.10 (EtOAc/*n*-hexanes/CH_3COOH 1/2/0.01); ^{1}H NMR (400 MHz, $CDCl_3$) δ 4.42 (s, 2 H, SC*H*$_2$), 4.60 (s, 2 H, SC*H*$_2$), 7.34 (dd, J_1 = 8.6 Hz, J_2 = 2.0 Hz, 1 H, Ar-*H*), 7.47–7.52 (m, 2 H, Ar-*H*), 7.54–7.59 (m, 3 H, Ar-*H*), 7.76 (d, J = 2.6 Hz, 1 H, Ar-*H*), 7.77 (d, J = 3.8 Hz, 1 H, Ar-*H*), 12.40 (br s, 1 H, N*H*); ^{1}H NMR (400 MHz, acetone-d_6) δ 4.51 (s, 2 H, SC*H*$_2$), 4.72 (s, 2 H, SC*H*$_2$), 7.41 (dd, J_1 = 8.6 Hz, J_2 = 2.1 Hz, 1 H, Ar-*H*), 7.63–7.71 (m, 4 H, Ar-*H*), 7.84 (s, 1 H, Ar-*H*), 7.99 (d, J = 8.6 Hz, 1 H, Ar-*H*), 8.03 (d, J = 2.0 Hz, 1 H, Ar-*H*); ^{13}C NMR (101 MHz, acetone-d_6) δ 28.08, 34.22, 122.49, 125.25 (q, $^1J_{F,C}$ = 271.3 Hz), 125.32, 125.76, 126.65 (q, $^3J_{F,C}$ = 3.7 Hz), 129.34, 129.80 (q, $^2J_{F,C}$ = 32.2 Hz), 130.76, 131.22, 131.34, 139.63, 140.28, 143.12, 153.97 (br s), 176.97 (br s); Purity by LC-MS: 96.2 %; HRMS (ESI) *m/z* calcd for $C_{20}H_{14}N_3OClF_3S_3$ $[M+H]^+$ 499.9934, found 499.9931.

4.1.8.12. 6-((3-(Bromomethyl)−5-chlorobenzo[b]thiophen-2-yl)thio)−4-((4-(trifluoromethyl)benzyl)thio)−1,3,5-triazin-2(1H)-one (33b). This compound was prepared according to the General procedure for the synthesis of 4,6-disubstituted 1,3,5-triazin-2(1*H*)-ones, starting from compound a mixture of compounds **21a** and **21b** (96 mg, 0.28 mmol [calc. for Mw of **21a**]) and 1-(bromomethyl)−4-(trifluoromethyl)benzene (74 mg, 0.31 mmol). Compound was separated from **33** and purified by column chromatography using EtOAc/*n*-hexanes/CH_3COOH (1/2/0.01) as an eluent system to give **33b** (39 mg, 24 % yield) as a white solid. *Note: this compound was not evaluated in biochemical assays due to*

the high reactivity of the bromomethyl moiety. R_f: 0.14 (EtOAc/*n*-hexanes/CH_3COOH 1/2/0.01); ^1H NMR (400 MHz, $CDCl_3$) δ 4.44 (s, 2 H, CH_2), 4.65 (s, 2 H, CH_2), 7.33 (dd, J_1 = 8.6 Hz, J_2 = 2.0 Hz, 1 H, Ar-*H*), 7.49–7.53 (m, 2 H, Ar-*H*), 7.56–7.60 (m, 2 H, Ar-*H*), 7.64 (d, J = 8.6 Hz, 1 H, Ar-*H*), 7.84 (d, J = 2.0 Hz, 1 H, Ar-*H*), 12.10 (br s, 1 H, N*H*); ^1H NMR (400 MHz, DMSO-d_6) δ 4.47 (s, 2 H, CH_2), 4.63 (s, 2 H, CH_2), 7.47 (dd, J_1 = 8.6 Hz, J_2 = 2.1 Hz, 1 H, Ar-*H*), 7.62–7.70 (m, 4 H, Ar-*H*), 8.03 (d, J = 8.7 Hz, 1 H, Ar-*H*), 8.05 (d, J = 2.1 Hz, 1 H, Ar-*H*), 13.12 (br s, 1 H, N*H*); ^{13}C NMR (101 MHz, DMSO-d_6) δ 26.51, 30.02, 118.73, 121.76, 124.04 (q, $^1J_{F,C}$ = 271.3 Hz), 124.23, 125.33 (q, $^3J_{F,C}$ = 3.7 Hz), 125.38, 127.88 (q, $^2J_{F,C}$ = 32.2 Hz), 129.54, 129.81, 130.50, 137.42, 138.31, 142.19, 153.33 (br s), 174.74 (br s); Purity by UHPLC: 97.9 %; HRMS (ESI) *m/z* calcd for $C_{20}H_{11}N_3OClBrF_3S_3$ $[M–H]^-$ 575.8894, found 575.8894.

4.1.8.13. 4-((3-Fluoro-5-(trifluoromethyl)benzyl)thio)− 6-((3-(trifluoromethyl)benzyl)thio)− 1,3,5-triazin-2(1 H)-one (34). This compound was prepared according to the General procedure for the synthesis of 4,6-disubstituted 1,3,5-triazin-2(1*H*)-ones, starting from compound **22** (65 mg, 0.20 mmol) and 1-(bromomethyl)−3-fluoro-5-(trifluoromethyl)benzene (57 mg, 0.22 mmol). Compound **34** was sufficiently pure after washing of the precipitate with *n*-hexanes. Off-white solid; yield, 72 % (71 mg); R_f: 0.26 (EtOAc/*n*-hexanes 1/1); ^1H NMR (400 MHz, DMSO-d_6) δ 4.43 (s, 4 H, 2 × SCH_2), 7.51–7.64 (m, 4 H, Ar-*H*), 7.65–7.68 (m, 1 H, Ar-*H*), 7.70 (d, J = 7.7 Hz, 1 H, Ar-*H*), 7.75–7.79 (m, 1 H, Ar-*H*), 13.05 (br s, 1 H, N*H*); ^{13}C NMR (101 MHz, DMSO-d_6) δ 32.99, 33.36, 112.17 (dq, $^2J_{F,C}$ = 23.4 Hz, $^3J_{F,C}$ = 3.5 Hz), 120.62 (d, $^2J_{F,C}$ = 22.3 Hz), 122.53 (q, $^3J_{F,C}$ = 3.7 Hz), 123.59 (qd,$^1J_{F,C}$ = 272.5 Hz, $^4J_{F,C}$ = 3.8 Hz), 124.50 (q, $^1J_{F,C}$ = 272.5 Hz), 124.51 (q, $^3J_{F,C}$ = 4.0 Hz), 126.13 (q, $^3J_{F,C}$ = 4.1 Hz), 129.55 (d, $^2J_{F,C}$ = 31.4 Hz), 129.98, 131.30 (qd, $^2J_{F,C}$ = 32.7 Hz, $^3J_{F,C}$ = 8.7 Hz), 133.60, 139.16, 142.62 (d, $^3J_{F,C}$ = 7.9 Hz), 150.39, 153.68 (br s), 162.21 (d, $^1J_{F,C}$ = 246.7 Hz), 179.33 (br s); Purity by UHPLC: 97.1 %; HRMS (ESI) *m/z* calcd for $C_{19}H_{13}N_3OF_7S_2$ $[M+H]^+$ 496.0383, found 496.0378.

4.1.8.14. 4-((3-Fluoro-5-(trifluoromethyl)benzyl)thio)−6-(((2-methylthiazol-4-yl)methyl)thio)−1,3,5-triazin-2(1H)-one (35). This compound was prepared according to the General procedure for the synthesis of 4,6-disubstituted 1,3,5-triazin-2(1*H*)-ones, starting from compound **23** (140 mg, 0.51 mmol) and 1-(bromomethyl)−3-fluoro-5-(trifluoromethyl)benzene (145 mg, 0.57 mmol). Compound **35** was sufficiently pure after washing of the precipitate with *n*-hexanes. White solid; yield, 59 % (135 mg); R_f: 0.22 (CH_2Cl_2/MeOH 20/1); ^1H NMR (400 MHz, DMSO-d_6) δ 2.61 (s, 3 H, CH_3), 4.41 (s, 2 H, SCH_2), 4.46 (s, 2 H, SCH_2), 7.36 (s, 1 H, Ar-*H*), 7.57–7.64 (m, 2 H, Ar-*H*), 7.68–7.71 (m, 1 H, Ar-*H*); ^{13}C NMR (101 MHz, DMSO-d_6) δ 18.69, 29.56, 32.56, 111.74 (dq, $^2J_{F,C}$ = 24.8 Hz, $^3J_{F,C}$ = 3.5 Hz), 116.91, 120.21 (d, $^2J_{F,C}$ = 22.0 Hz), 122.02 (q, $^3J_{F,C}$ = 3.9 Hz), 123.09 (qd, $^1J_{F,C}$ = 271.6 Hz, $^4J_{F,C}$ = 3.8 Hz), 130.87 (qd, $^2J_{F,C}$ = 32.7 Hz, $^3J_{F,C}$ = 8.6 Hz), 142.20 (d, $^3J_{F,C}$ = 8.0 Hz), 149.84, 149.94, 153.34 (br s), 161.80 (d, $^1J_{F,C}$ = 246.5 Hz), 165.82, 175.40 (br s); Purity by LC-MS: 95.8 %; HRMS (ESI) *m/z* calcd for $C_{16}H_{12}ON_4F_4S_3$ $[M+H]^+$ 449.0182, found 449.0183.

4.1.8.15. 6-(((2-Methylthiazol-4-yl)methyl)thio)−4-((4-(trifluoromethyl)benzyl)thio)−1,3,5-triazin-2(1H)-one (36). This compound was prepared according to the General procedure for the synthesis of 4,6-disubstituted 1,3,5-triazin-2(1*H*)-ones, starting from compound **23** (140 mg, 0.51 mmol) and 1-(bromomethyl)−4-(trifluoromethyl)benzene (136 mg, 0.57 mmol). Compound **36** was sufficiently pure after washing of the precipitate with *n*-hexanes. White solid; yield, 56 % (123 mg); R_f: 0.42 (CH_2Cl_2/MeOH 9/1); ^1H NMR (400 MHz, DMSO-d_6) δ 2.61 (s, 3 H, CH_3), 4.41 (s, 2 H, SCH_2), 4.46 (s, 2 H, SCH_2), 7.36 (s, 1 H, Ar-*H*), 7.63 (app d, J = 8.2 Hz, 2 H, Ar-*H*), 7.69 (app d, J = 8.2 Hz, 2 H, Ar-*H*), 12.91 (br s, 1 H, N*H*); ^{13}C NMR (101 MHz, DMSO-d_6) δ 18.72, 20.60, 32.95, 116.92, 124.22 (q, $^1J_{F,C}$ = 271.7 Hz), 125.37 (q, $^3J_{F,C}$ = 3.7 Hz), 127.88 (q, $^2J_{F,C}$ = 31.6 Hz), 129.79, 142.22, 149.92, 149.96, 153.43 (br s), 165.85, 174.83 (br s); Purity by UHPLC: 96.5 %; HRMS (ESI) *m/z* calcd for $C_{16}H_{13}ON_4F_3S_3$ $[M+H]^+$ 431.0276, found 431.0278.

4.1.8.16. 4-((4-Isopropylbenzyl)thio)−6-(((2-methylthiazol-4-yl)methyl)thio)−1,3,5-triazin-2(1H)-one (37). This compound was prepared according to the General procedure for the synthesis of 4,6-disubstituted 1,3,5-triazin-2(1*H*)-ones, starting from compound **23** (140 mg, 0.51 mmol) and 1-(bromomethyl)−4-isopropylbenzene (121 mg, 0.57 mmol). Compound **37** was sufficiently pure after washing of the precipitate with *n*-hexanes. White solid; yield, 83 % (172 mg); R_f: 0.37 (CH_2Cl_2/MeOH 9/1); ^1H NMR (400 MHz, DMSO-d_6) δ 1.18 (d, J = 6.8 Hz, 6 H, Ar-CH(CH_3)$_2$), 2.62 (s, 3 H, CH_3), 2.85 (sept, J = 6.9 Hz, 1 H, Ar-C*H*(CH$_3$)$_2$), 4.34 (s, 2 H, SCH_2), 4.42 (s, 2 H, SCH_2), 7.17–7.22 (m, 2 H, Ar-*H*), 7.28–7.33 (m, 2 H, Ar-*H*), 7.36 (s, 1 H, Ar-*H*), 12.66 (br s, 1 H, N*H*); ^{13}C NMR (101 MHz, DMSO-d_6) δ 18.75, 23.86, 29.66, 33.15, 33.44, 116.89, 126.53, 129.05, 139.95, 147.72, 149.97, 150.04, 153.32 (br s), 165.86, 172.42 (br s); Purity by LC-MS: 96.2 %; HRMS (ESI) *m/z* calcd for $C_{18}H_{20}ON_4S_3$ $[M+H]^+$ 405.0872, found 405.0873.

4.2. Human topo IIα-mediated decatenation assay

Assays described in Section 4.2. to 4.7. were performed in collaboration with Inspiralis (Norwich, UK) with methodologies and procedures already applied in our past studies of catalytic topo IIα inhibitors [51, 52]. All assays were performed in duplicates. More assay details are provided in Section 2 of the Supplementary material.

Topo IIα-mediated decatenation assay was performed for all compounds at concentrations 7.8, 15.6, 31.25, 125 μM and, additionally at 0.78, 1.95, 7.8, 15.6, and 31.25 μM for compound **37**, as well as 0.12, 0.49, 1.95, and 7.8 for compounds **32** and **33** with etoposide as a control compound at concentrations 7.8, 15.6, 31.25, 125 μM. IC_{50} values were calculated with GraphPad Prism 9.5.0 [53].

4.3. Human topo IIβ-mediated decatenation assay

This assay was performed in duplicates for compounds **24, 30, 32** and **37** at concentrations 7.8, 15.6, 31.25, 125 μM and at concentrations 1.95, 7.8, 15.6, 31.25, 125 μM of compound **32** along with etoposide as a control compound. More assay details are provided in Section 3 of the Supplementary material.

4.4. Human topoisomerase IIα-mediated relaxation assay

Topo IIα-mediated relaxation assay was performed at four different concentrations of compounds **32, 33** (1.95, 7.8, 15.6 and 31.25 μM), compounds **24**, **30** (7.8, 15.6, 31.25, and 62.5 μM), compound **37** (31.25, 62.5, 125 and 500 μM) and of etoposide as positive control (10 and 100 μM). More assay details are provided in Section 4 of the Supplementary material.

4.5. Human topoisomerase IIα-mediated cleavage and competitive cleavage assay

The cleavage assay was performed for compounds **24, 30, 31, 32**, and **37** at concentrations 7.8, 15.6, 31.25, 125 μM and etoposide as a control compound. The competitive cleavage assay used the same four concentrations of compounds **24** and **30**, with the main difference that a constant etoposide concentration of 50 μM of etoposide was present. Total DMSO in the assay was 2 % (cumulative effect of adding 2 different compounds). More assay details are provided in Sections 5 and

6 of the Supplementary material.

4.6. Wheatgerm topo I unwinding assay

An unwinding assay was performed for compounds **24, 30** and **37** at concentrations of 7.8, 15.6, 31.25, and 125 μM and mAMSA as a control compound. More assay details are provided in Section 7 of the Supplementary material.

4.7. Competitive ATPase assay

This assay was performed at 9 different concentrations of the ATP (0.025, 0.05, 0.075, 0.1, 0.25, 0.5, 0.75, 1, and 2 mM) and at concentration 1.95, 3.9, 7.8, 15.6 μM for compound **24**, and at 7.8, 15.6, 31.25, and 125 μM for compounds **30**. The final DMSO concentration in all the reactions was 5 % (v/v).

Compounds **24** and **30** were dissolved and diluted in DMSO and added to the reaction before the addition of the enzyme. Compounds were analyzed using a linked ATPase assay in which the ADP produced by the hydrolysis of ATP leads to the conversion of NADH to NAD by a pyruvate kinase/lactate dehydrogenase mix. The disappearance of NADH was monitored at 340 nm. Assay was performed in duplicates [54].

A mix of assay buffer (5 μl of 10X buffer per assay: final conc. 20 mM Tris-HCl, 5 mM magnesium acetate, 125 mM potassium acetate, 2 mM DTT, pH 7.9), linear pBR322 (1.5 μl of 1 mg/mL per assay), phosphoenol pyruvate (0.5 μl of 80 mM per assay), pyruvate kinase/lactate dehydrogenase mix (0.75 μl per assay), NADH (1 μl of 20 mM per assay) and water (32.35 μl per assay) was made. 39.1 μl was aliquoted into the wells of a 384-well microtitre plate. 2.5 μl of DMSO or the appropriate compound were added to the wells and mixed. 5 μl of the dilution buffer or human topo II (140 nM stock giving 14 nM final concentration) were then added and mixed. The change in OD340 was then measured in a plate reader over a period of about 10–15 min (called the pre-run). 3.4 μl of 30 mM ATP was then added and the OD340 monitored for up to 30 min. Assays were performed at 37 °C. More assay details are provided in Section 8 of the Supplementary material.

4.8. STD NMR spectroscopy experiments

High-resolution NMR spectra were recorded on Bruker Avance Neo 600 MHz Spectrometer, using cryoprobes, at 25 °C. Data were collected using the pulse sequences provided by the Bruker library of pulse programs and analyzed with Bruker Topspin 4.2.0. The residual water signal was suppressed using excitation sculpting [55] with 2 ms selective pulse (or 5 ms selective pulse for STD and reference spectra of compound **37**). $T_1\rho$ filter of 100 ms was used to eliminate the background protein resonances. ATPase domain of topo IIα protein was purchased from Inspiralis, UK. The ^{1}H spectral widths were 6250 Hz (compounds **30**, **31**, and **24**) or 5882 Hz (compound **37**) (Section 9 of Supplementary Information). NMR samples were prepared in a buffer 20 mM Na-phosphate (pD 7.7), 150 mM KCl, 5 mM $MgCl_2$ in D_2O, complemented with 10 % DMSO-d_6 and 0.02 % NaN_3. The complete assignment of protons was achieved using a combination of COSY, TOCSY and HSQC spectra (Tables S16 – S23). The ^{1}H STD and trNOESY spectra were recorded at a protein:ligand ratio of 1:100, where the protein concentration was 1 μM, and the ligand concentration was 0.1 mM.

The ^{1}H STD ligand epitope mapping experiments [39] were performed with 16 384 (compound **30**, **31**, **24**) or 65 536 (compound **37**) data points, a relaxation delay of 4 s (compounds **30**, **31**, **24**) or 1.5 s (compound **37**), and 5440 (compound **30**, **31**, **24**) or 5040 (compound **37**) scans. In the case of compounds **30**, **31** and **24** the short protein saturation time of 0.5 s was used to avoid the influence of relaxation on STD amplification factors [56]. In the case of **37,** the saturation time of 1 s was used to increase signal-to-noise ratio and consequently to decrease errors of STD amplification factors for individual protons below 10 %. The on-resonance selective saturation of topo II was applied at − 0.727 ppm at transmitter offset referenced to 4.70 ppm. The off-resonance irradiation was applied at 30 ppm for the reference spectrum. Spectra were zero-filled and apodized by an exponential line-broadening function of 3 Hz. Errors in the STD amplification factor were estimated according to the formula [57]:

$$\text{STD amplification factor absolute error} = \text{STD amplification factor} \times [(\frac{N_{STD}}{I_{STD}})^2 + (\frac{N_{REF}}{I_{REF}})^2)]^{\frac{1}{2}}$$

N_{STD} and N_{REF} are noise levels in STD and reference spectra. I_{STD} and I_{REF} are signal intensities in STD and reference spectra. Relative errors of amplification factors for all protons are under 1 % (compound **30**), 3 % (compounds **31, 24**) and 5 % (**37**).

4.9. Inhibition of human protein kinases

Inhibition effect of compound **24** on a selected set of human protein kinases was performed with *KinaseProfiler*^{TM} (Eurofins Cerep SA, Celle-L'Evescault, France) which are kinase activity radiometric assays. Compound was prepared to 50x final assay concentration in 100 % DMSO. The tested compound concentration was 10 μM. The working stock of each compound was added to the assay well as the first component in the reaction, followed by the remaining components as detailed in the general assay protocols (Table 4).

In the *KinaseProfiler*^{TM} there is no pre-incubation step between the compound and the human protein kinase prior to start of the reaction. The positive control wells contain all components of the reaction, except the compound of interest; however, DMSO at a final concentration of 2 % is included in these wells to control for solvent effects. The blank wells contain all reaction components and a reference kinase inhibitor replacing the compound of interest which completely abolishes the kinase activity and establishes the baseline corresponding to 0 % kinase activity. The used known inhibitors used to generate the blank signal for each tested protein kinase are listed in Table 5. Complete descriptions of protocols used to evaluate inhibition activity of each selected human protein kinase are available in Section 13 of Supplementary material.

Table 4
Buffer compositions for the preparation of human protein kinases before their addition to the reaction mix.

Buffer Composition	Protein Kinase (s)
20 mM MOPS, 1 mM EDTA, 0.01 % Brij-35, 5 % Glycerol, 0.1 % β- mercaptoethanol, 1 mg/mL BSA	CDK1/cyclinB, c-Kit, EGFR, FGFR1, FGFR3, Flt1, Flt3, Fms, JAK2, PDGFRα, PKA, PKBα, Ret, Src (1-530)
45 mM TRIS, 0.4 mM EGTA, 18 mM DTT, 0.02 % Triton X-100, 1 mM sodium orthovandate, 1 mM β-glycerophosphate, 2 % glycerol	B-Raf, c-Raf
50 mM TRIS, 0.1 mM EGTA, 0.1 mM Na3VO4, 0.1 % β- mercaptoethanol, 1 mg/mL BSA	IGF-1R
50 mM HEPES, 1 mM EDTA, 10 mM DTT, 0.01 % Brij-35	MEKK3

Table 5
Selection of reference kinase inhibitors and their targeted human protein kinases.

Reference kinase Inhibitor	Protein Kinase (s)
PI-103	DNA-PK
KU55933	ATM
Staurosporine	B-Raf, CDK1/cyclinB, cKit, c-Raf, EGFR, FGFR1, FGFR3, Flt1, Flt3, Fms, IGF-1R, JAK2, MEKK3, PDGFRα, PKA, PKBα, Ret, Src(1-530)

4.10. Molecular docking calculations

Molecular docking was performed with GOLD software [58] and protomer (chain A) of the human topo IIα ATPase domain (PDB: 1ZXM) and protomer (chain A) of the human topo IIβ ATPase domain (PDB: 7QFO) (Fig. S16) [24]. With the docking settings described below which are largely based on our previous studies [51,59] we first redocked the AMP-PNP native ligand in both topo IIα and topo IIβ ATP binding sites (Fig. S17). The actives sites were defined as a 6 Å radius around the bound ANP-PNP ligands. Crystal waters W924 and W931 present in topoi IIα were included in docking as they play an important role in binding of the native molecule. The same was done for topo IIβ with inclusion of crystal W644 and W670. For included waters different spin states were allowed during docking calculations [21]. GOLD genetic algorithm (GA) was used as a search algorithm with the default settings and the GoldScore scoring function ranked the compounds. To ensure similar interaction pattern of the 1,3,5-triazin-2(1*H*)-one's scaffold with ATP site, an H-bond constraint was added to Asn120 (topo IIα) [21] and Asn136 (topo IIβ). Docking calculations were visualized and geometrically analyzed in LigandScout [60].

4.11. Structure-based lead optimization with Deepfrag

The DeepFrag software enables structure-based optimization of compounds and is based on deep learning architecture and is accessible via an on-line interface [22,23]. Here, we loaded separately a protomer (chain A) of ATPase domain of human topo IIα (PDB: 1ZXM) and docked conformation of triazinone, with 3-chlorophenyl substituent at position 6 and optimized substituent 3-trifluoromethyl-5-fluorobenzyl at position 4. We removed the substituent at the 6 position and chose the carbon atom adjacent to sulfur as the growth point and used default settings for the search (Fig. S1). DeepFrag displayed the list of most favorable fragments that could be introduced based on the favorability of the interactions and topological constraints of the ATP pocket. The fragments were ranked according to the favorability of interactions assessed by an internal scoring function and the more favorable are listed in Table S1.

4.12. Molecular dynamics simulations

The starting complexes for molecular simulations were derived from molecular docking in the monomer A of the topo IIα ATP binding site. Together four complexes were simulated, the first complex with 9H-purine preclinical compound **QAP 1** and three designed 4,6-substituted-1,3,5-triazin-2(1*H*)-ones: compound **31** (**model**) compound, and R^1 monocylclic and bicyclic compounds **24** and **37**. More details on MD simulation results of compound **37** are provided in Section 11 of the Supplementary material.

For ligands **QAP 1**, **24** and **31** and **37** force field parameters were determined. Partial charges were determined with a standard Merz-Kollman scheme on the geometry optimized structures at the Hartree–Fock level using the 6–31 G* basis set. Gaussian 16 was employed for the QM optimization [61] and RESP charges generation was performed with Amber20 [62]. Ligand force field parameters were obtained in Antechamber module, using input bond lengths and bond angles obtained from the QM optimized geometries. General Amber Force Field of second generation (GAFF2) was used for the description of ligands (Section 14 of the Supplementary Information, Tables S25 – S28) [63]. The systems were solvated with TIP3P water molecules and three Cl-couterions were added to make the system electroneutral [64]. The final systems comprised around 33,000 atoms and Amber14SB force field for the protein [65] and GAFF2 for ligands description [63].

On these systems we conducted a 10,000-step steepest descent energy minimization, followed by a 20,000-step conjugate gradient optimization. The NVT equilibration involved four runs, each with 10,000 steps and a 2 fs time step, gradually releasing constraints on the protein. The force constant for the first run was 100 kcal/mol $Å^{-2}$, second 60 kcal/mol $Å^{-2}$, third 30 kcal/mol $Å^{-2}$ and fourth was without restraint. Heating to 300 K was achieved during NVT equilibration, controlled by the Langevin thermostat [66]. The NPT equilibration consisted of two runs with 100,000 steps and a 2 fs time step, with the first run constraining the topo II ATPase domain with the force constant of 20 kcal/mol $Å^{-2}$and the second run without constraints while NPT equilibration maintained a pressure of 1 bar using the Berendsen barostat [67]. Long-range electrostatics were treated with Particle Mesh Ewald [68], and periodic boundary conditions were applied. The SHAKE algorithm [69] constrained hydrogen bond lengths, achieving a 2 fs time step. Each system underwent 0.5 microseconds of MD simulation using Amber20 program [62]. MD simulation trajectories were analyzed with approaches outlined below. For visualizations we used VMD [70], PyMOL [71] and UCSF Chimera [72] software.

The *Cpptraj* module [73] calculated RMSD across the entire trajectories of all simulated compounds. RMSD values were computed with reference to the initial structures of the protein and ligand, respectively. To offer a more comprehensive understanding of the dynamic interaction pattern between the ligands in the ATP binding site the dynophore calculations were performed using DynophoreApp [74]. 2000 equidistant frames from the MD simulation were analyzed and the resulting dynophore model underwent further analysis. These calculations were carried out on computers at the Molecular Design Lab in Germany and later visualized in LigandScout [60]. The protein-ligand complexes' binding free energy was assessed through calculations using the MM/GBSA free energy calculations incorporated in Amber 22 [73,75] with MMPBSA.py [76] on equidistant 350 snapshots extracted from the final 450 ns of the MD simulations of the trajectories of each ligand, representing a fully equilibrated simulated system. The Generalized Born IGB method 5 and a 0.10 M salt concentration were employed. Additionally, per-residue decomposition was performed to assess the energy contributions of individual residues to the binding process.

4.13. NCI-60 screening of human tumor cell lines

The National Cancer Institute (NCI) evaluated the compounds on a set of 60 human cancer cell lines. The full list of used human cell lines can be found on the NCI website [77]. The testing procedure involved fixing cells with trichloroacetic acid, followed by staining with sulforhodamine B (SRB) and measuring absorbance. Additional details on methodology in [78]. Compounds were assessed at a concentration of 10 μM and the NCS codes for the assays are 832727 (compound **24**), 832729 (compound **25**), and 832728 (compound **26**), 842916 (compound **34**), 842915 (compound **37**). Results are presented as growth values relative to the control without the compound and in relation to the cell count at the start, and this allowed the determination of no inhibition of growth (values between 0 and 100) and lethality (values between −100 and 0) [78]. More details on NCI-60 screening results performed on compounds **26** and **34** is available in Section 12 of the Supplementary material.

CRediT authorship contribution statement

B.H. and A.P. performed molecular design; N.S.B and I.S. were involved in the synthesis of the targeted molecules; B.H. performed molecular simulations; B.H. and A.P. analyzed the results of the computational studies; T.G and S.G.G. performed STD NMR measurements; A.P. conceptualized and supervised the research and provided funding. All authors were involved in the writing and editing of the manuscript.

Declaration of Competing Interest

The authors declare no competing interest.

Acknowledgments

This work was supported by the Slovenian Research and Innovation Agency (ARIS) through research projects J1–4402 (A.P.) and J1–4400 (S.G.G.) and research programs P1-0012, P1-0010 and P1-0208 as well as a young researcher funding to B.H. Dr. Nicolas Burton and Dr. Alison Howells from Inspiralis, Norwich, UK are acknowledged for expressing and isolating the ATPase domain of human topo IIα as well as performing topoisomerase IIα relaxation, decatenation, cleavage, competitive cleavage, competitive ATPase and unwinding assays. Master students Aljoša Korošec, Anja Pavlovič and Gašper Grošelj are acknowledged for their contribution to the synthesis of compounds discussed in this work. Prof. Gerhard Wolber is thanked for providing access to dynophore calculations at the computer cluster of the Freie Universität Berlin, Germany. We recorded NMR spectra on NMR spectrometers of the Slovenian NMR Centre at the National Institute of Chemistry, Ljubljana. We acknowledge Ažman high-performance computing (HPC) center at the National Institute of Chemistry for computational resources and National Cancer Institute, USA for performing the assays within their NCI-60 program.

Supplementary material

Supplementary Information includes: (1) Supporting figures, tables, and graphs (pdf file), (2) Coordinates of the starting structures for molecular simulation (zip file) (3) Animations of the derived dynamical pharmacophore model of hit compound **QAP 1** and compound **31** depicted on the obtained trajectory (mp4 file).

Appendix A. Supporting information

Supplementary data associated with this article can be found in the online version at doi:10.1016/j.csbj.2024.06.037.

References

[1] National Cancer Institute, ⟨https://www.cancer.gov/about-cancer/understanding/statistics⟩, 13.02.2023.
[2] Siegel RL, Miller KD, Fuchs HE, Jemal A. Cancer statistics, 2021. CA Cancer J Clin 2021;71:7–33.
[3] Hanahan D, Weinberg RA. The hallmarks of cancer. Cell 2000;100:57–70.
[4] World Health Organization: Cancer, ⟨https://www.who.int/news-room/fact-sheets/detail/cancer⟩, 23. 11. 2023).
[5] Deweese JE, Osheroff MA, Osheroff N. DNA topology and topoisomerases: teaching a "knotty" subject. Biochem Mol Biol Educ 2008;37:2–10.
[6] Pommier Y, Leo E, Zhang HL, Marchand C. DNA topoisomerases and their poisoning by anticancer and antibacterial drugs. Chem Biol 2010;17:421–33.
[7] Nitiss JL. DNA topoisomerase II and its growing repertoire of biological functions. Nat Rev Cancer 2009;9:327–37.
[8] Hanahan D, Weinberg RA. Hallmarks of cancer: the next generation. Cell 2011;144:646–74.
[9] Pogorelčnik B, Perdih A, Solmajer T. Recent advances in the development of catalytic inhibitors of human DNA topoisomerase IIα as novel anticancer agents. Curr Med Chem 2013;20:694–709.
[10] Nitiss JL. Investigating the biological functions of DNA topoisomerases in eukaryotic cells. Biochim Biophys Acta 1998;1400:63–81.
[11] Wang JC. Cellular roles of DNA topoisomerases: A molecular perspective. Nat Rev Mol Cell Bio 2002;3:430–40.
[12] Fortune JM, Osheroff N. Topoisomerase II as a target for anticancer drugs: When enzymes stop being nice. Prog Nucleic Acid ReS 2000;64:221–53.
[13] Pogorelčnik B, Perdih A, Solmajer T. Recent developments of DNA poisons - human DNA topoisomerase IIα inhibitors - as anticancer agents. Curr Pharm Des 2013;19:2474–88.
[14] Hu W, Huang XS, Wu JF, Yang L, Zheng YT, Shen YM, Li ZY, Li X. Discovery of novel topoisomerase II inhibitors by medicinal chemistry approaches. J Med Chem 2018;61:8947–80.
[15] Minotti G, Menna P, Salvatorelli E, Cairo G, Gianni L. Anthracyclines: Molecular advances and pharmacologic developments in antitumor activity and cardiotoxicity. Pharm Rev 2004;56:185–229.
[16] Felix CA. Secondary leukemias induced by topoisomerase-targeted drugs. Biochim Biophys Acta 1998;1400:233–55.
[17] Chene P, Rudloff J, Schoepfer J, Furet P, Meier P, Qian Z, Schlaeppi JM, Schmitz R, Radimerski T. Catalytic inhibition of topoisomerase II by a novel rationally designed ATP-competitive purine analogue. BMC Chem Biol 2009;9:1.
[18] Vanden Broeck A, Lotz C, Drillien R, Haas L, Bedez C, Lamour V. Structural basis for allosteric regulation of Human Topoisomerase IIα. Nat Commun 2021;12:2962.
[19] Pogorelčnik B, Brvar M, Zajc I, Filipič M, Solmajer T, Perdih A. Monocyclic 4-amino-6-(phenylamino)-1,3,5-triazines as inhibitors of human DNA topoisomerase IIα. Bioorg Med Chem Lett 2014;24:5762–8.
[20] Pogorelčnik B, Janežič M, Sosič I, Gobec S, Solmajer T, Perdih A. 4,6-Substituted-1,3,5-triazin-2(1H)-ones as monocyclic catalytic inhibitors of human DNA topoisomerase IIα targeting the ATP binding site. Bioorg Med Chem 2015;23:4218–29.
[21] Bergant K, Janežic M, Valjavec K, Sosič I, Pajk S, Štampar M, Žegura B, Gobec S, Filipič M, Perdih A. Structure-guided optimization of 4,6-substituted-1,3,5-triazin-2(1H)-ones as catalytic inhibitors of human DNA topoisomerase IIα. Eur J Med Chem 2019;175:330–48.
[22] Green H, Koes DR, Durrant JD. DeepFrag: a deep convolutional neural network for fragment-based lead optimization. Chem Sci 2021;12:8036–47.
[23] Green H, Durrant JD. DeepFrag: an open-source browser app for deep-learning lead optimization. J Chem Inf Model 2021;61:2523–9.
[24] Wei H, Ruthenburg AJ, Bechis SK, Verdine GL. Nucleotide-dependent domain movement in the ATPase domain of a human type IIA DNA topoisomerase. J Biol Chem 2005;280:37041–7.
[25] Furet P, Schoepfer J, Radimerski T, Chene P. Discovery of a new class of catalytic topoisomerase II inhibitors targeting the ATP-binding site by structure based design. Part I. Bioorg Med Chem Lett 2009;19:4014–7.
[26] Schaller D, Šribar D, Noonan T, Deng L, Nguyen TN, Pach S, Machalz D, Bermudez M, Wolber G. Next generation 3D pharmacophore modeling. WIREs Comput Mol Sci 2020;10:e1468.
[27] Buonfiglio R, Recanatini M, Masetti M. Protein flexibility in drug discovery: from theory to computation. Chem Med Chem 2015;10:1141–8.
[28] Salmaso V, Moro S. Bridging molecular docking to molecular dynamics in exploring ligand-protein recognition process: an overview. Front Pharm 2018;9:923.
[29] Bender A, Cortes-Ciriano I. Artificial intelligence in drug discovery: what is realistic, what are illusions? Part 1: Ways to make an impact, and why we are not there yet. Drug Discov Today 2021;26:511–24.
[30] LeCun Y, Bengio Y, Hinton G. Deep learning. Nature 2015;521:436–44.
[31] Sosič I, Mirković B, Turk S, Štefane B, Kos J, Gobec S. Discovery and kinetic evaluation of 6-substituted 4-benzylthio-1,3, 5-triazin-2(1*H*)-ones as inhibitors of cathepsin B. Eur J Med Chem 2011;46:4648–56.
[32] Toyoda E, Kagaya S, Cowell IG, Kurosawa A, Kamoshita K, Nishikawa K, Iiizumi S, Koyama H, Austin CA, Adachi N. NK314, a topoisomerase II inhibitor that specifically targets the α isoform. J Biol Chem 2008;283:23711–20.
[33] Sakaguchi A, Kikuchi A. Functional compatibility between isoform α and β of type II DNA topoisomerase. J Cell Sci 2004;117:1047–54.
[34] Skok Ž, Zidar N, Kikelj D, Ilaš J. Dual Inhibitors of Human DNA Topoisomerase II and Other Cancer-Related Targets. J Med Chem 2019.
[35] Plech T, Kapron B, Paneth A, Wujec M, Czarnomysy R, Bielawska A, Bielawski K, Trotsko N, Kusmierz E, Paneth P. Search for human DNA topoisomerase II poisons in the group of 2,5-disubstituted-1,3,4-thiadiazoles. J Enzym Inhib Med Chem 2015;30:1021–6.
[36] Karki R, Jun KY, Kadayat TM, Shin S, Thapa Magar TB, Bist G, Shrestha A, Na Y, Kwon Y, Lee ES. A new series of 2-phenol-4-aryl-6-chlorophenyl pyridine derivatives as dual topoisomerase I/II inhibitors: Synthesis, biological evaluation and 3D-QSAR study. Eur J Med Chem 2016;113:228–45.
[37] Park S, Kadayat TM, Jun KY, Thapa Magar TB, Bist G, Shrestha A, Lee ES, Kwon Y. Novel 2-aryl-4-(4′-hydroxyphenyl)-5H-indeno[1,2-b]pyridines as potent DNA non-intercalative topoisomerase catalytic inhibitors. Eur J Med Chem 2017;125:14–28.
[38] Georgiadis MM, Singh I, Kellett WF, Hoshika S, Benner SA, Richards NG. Structural basis for a six nucleotide genetic alphabet. J Am Chem Soc 2015;137:6947–55.
[39] Mayer M, Meyer B. Group epitope mapping by saturation transfer difference NMR to identify segments of a ligand in direct contact with a protein receptor. J Am Chem Soc 2001;123:6108–17.
[40] Villman K, Stahl E, Liljegren G, Tidefelt U, Karlsson MG. Topoisomerase II-α expression in different cell cycle phases in fresh human breast carcinomas. Mod Pathol 2002;15:486–91.
[41] van der Zee AG, de Vries EG, Hollema H, Kaye SB, Brown R, Keith WN. Molecular analysis of the topoisomerase IIα gene and its expression in human ovarian cancer. Ann Oncol 1994;5:75–81.
[42] Feng Y, Zhang H, Gao W, Wen S, Huangfu H, Sun R, Bai W, Wang B. Expression of DNA topoisomerase IIα: clinical significance in laryngeal carcinoma. Oncol Lett 2014;8:1575–80.
[43] Kellner U, Heidebrecht HJ, Rudolph P, Biersack H, Buck F, Dakowski T, Wacker HH, Domanowski M, Seidel A, Westergaard O, Parwaresch R. Detection of human topoisomerase IIα in cell lines and tissues: characterization of five novel monoclonal antibodies. J Histochem Cytochem 1997;45:251–63.
[44] The Human Protein Atlas, ⟨https://www.proteinatlas.org/ENSG00000131747-TOP2A/tissue⟩, 31. 01. 2024.
[45] Prazeres VF, Tizon L, Otero JM, Guardado-Calvo P, Llamas-Saiz AL, van Raaij MJ, Castedo L, Lamb H, Hawkins AR, Gonzalez-Bello C. Synthesis and biological evaluation of new nanomolar competitive inhibitors of Helicobacter pylori type II dehydroquinase. Structural details of the role of the aromatic moieties with essential residues. J Med Chem 2010;53:191–200.
[46] R. Nirogi, A.K. Shinde, A.R. Mohammed, R.K. Badange, P. Jayarajan, G. Bhyrapuneni, V. Jasti, Muscarinic m1 receptor positive allosteric modulators, (2020).WO2018042362A1.

[47] Ni S, El Remaily MAEAAA, Franzén J. Carbocation Catalyzed Bromination of Alkyl Arenes, a Chemoselective sp3vs. sp2C−H functionalization. Adv Synth Catal 2018; 360:4197–204.
[48] Bauer S, Ochoa-Puentes C, Sun Q, Bause M, Bernhardt G, Konig B, Buschauer A. Quinoline carboxamide-type ABCG2 modulators: indole and quinoline moieties as anilide replacements. Chemmedchem 2013;8:1773–8.
[49] Troester A, Alonso R, Bauer A, Bach T. Enantioselective Intermolecular [2 + 2] Photocycloaddition Reactions of 2(1H)-Quinolones Induced by Visible Light Irradiation. J Am Chem Soc 2016;138:7808–11.
[50] J.H. Hutchinson, P.P. Prasit, B.A. Stearns, J.F. Evans, M. Moran, Y. Li, B. Wang, Y. P. Truong, J.R. Roppe, J.M. Scott, J.E. Zunic, J.M. Arruda, T.J. Seiders, N.S. Stock, M. Haddach, 5-lipoxygenase-activating protein (flap) inhibitors, (2008). WO2008137609A1.
[51] Bergant Loboda K, Janežič M, Štampar M, Žegura B, Filipič M, Perdih A. Substituted 4,5′-bithiazoles as catalytic inhibitors of human DNA topoisomerase IIα. J Chem Inf Model 2020;60:3662–78.
[52] Janežič M, Valjavec K, Loboda KB, Herlah B, Ogris I, Kozorog M, Podobnik M, Grdadolnik SG, Wolber G, Perdih A. Dynophore-based approach in virtual screening: a case of human DNA topoisomerase IIα. Int J Mol Sci 2021;22:13474.
[53] GraphPad Software, GraphPad Prism Version 9 for Windows, ⟨www.graphpad.com⟩, 6. 1. 2024.
[54] Bergant K, Janežič M, Perdih A. Bioassays and *in silico* methods in the identification of human DNA topoisomerase IIα inhibitors. Curr Med Chem 2018;25:3286–318.
[55] Hwang TL, Shaka AJ. Water suppression that works. Excitation sculpting using arbitrary wave-forms and pulsed-field gradients. J Magn Reson, Ser A 1995;112: 275–9.
[56] Yan J, Kline AD, Mo H, Shapiro MJ, Zartler ER. The effect of relaxation on the epitope mapping by saturation transfer difference NMR. J Magn Reson 2003;163: 270–6.
[57] McCullough C, Wang M, Rong L, Caffrey M. Characterization of influenza hemagglutinin interactions with receptor by NMR. PLoS One 2012;7:e33958.
[58] Jones G, Willett P, Glen RC, Leach AR, Taylor R. Development and validation of a genetic algorithm for flexible docking. J Mol Biol 1997;267:727–48.
[59] Ogrizek M, Janežič M, Valjavec K, Perdih A. Catalytic mechanism of ATP hydrolysis in the ATPase domain of human DNA topoisomerase IIα. J Chem Inf Model 2022;62:3896–909.
[60] Wolber G, Langer T. LigandScout: 3-D pharmacophores derived from protein-bound ligands and their use as virtual screening filters. J Chem Inf Model 2005;45: 160–9.
[61] Frisch MJ, Trucks GW, Schlegel HB, Scuseria GE, Robb MA, Cheeseman JR, Scalmani G, Barone V, Petersson GA, Nakatsuji H, Li X, Caricato M, Marenich AV, Bloino J, Janesko BG, Gomperts R, Mennucci B, Hratchian HP, Ortiz JV, Izmaylov AF, Sonnenberg JL, Williams, Ding F, Lipparini F, Egidi F, Goings J, Peng B, Petrone A, Henderson T, Ranasinghe D, Zakrzewski VG, Gao J, Rega N, Zheng G, Liang W, Hada M, Ehara M, Toyota K, Fukuda R, Hasegawa J, Ishida M, Nakajima T, Honda Y, Kitao O, Nakai H, Vreven T, Throssell K, Montgomery Jr JA, Peralta JE, Ogliaro F, Bearpark MJ, Heyd JJ, Brothers EN, Kudin KN, Staroverov VN, Keith TA, Kobayashi R, Normand J, Raghavachari K, Rendell AP, Burant JC, Iyengar SS, Tomasi J, Cossi M, Millam JM, Klene M, Adamo C, Cammi R, Ochterski JW, Martin RL, Morokuma K, Farkas O, Foresman JB, Fox DJ. C.01, in, Wallingford, CT. 16 Rev..,. Gaussian,; 2016.
[62] D.A. Case, K. Belfon, I.Y. Ben-Shalom, S.R. Brozell, D.S. Cerutti, I.T.E. Cheatham, V. W.D. Cruzeiro, T.A. Darden, R.E. Duke, G. Giambasu, M.K. Gilson, H. Gohlke, A.W. Goetz, R. Harris, S. Izadi, S.A. Izmailov, K. Kasavajhala, A. Kovalenko, R. Krasny, T. Kurtzman, T.S. Lee, S. LeGrand, P. Li, C. Lin, J. Liu, T. Luchko, R. Luo, V. Man, K.M. Merz, Y. Miao, O. Mikhailovskii, G. Monard, H. Nguyen, A. Onufriev, F.Pan, S. Pantano, R. Qi, D.R. Roe, A. Roitberg, C. Sagui, S. Schott-Verdugo, J. Shen, C.L. Simmerling, N.R.Skrynnikov, J. Smith, J. Swails, R.C. Walker, J. Wang, L. Wilson, R.M. Wolf, X. Wu, Y. Xiong, Y. Xue, D.M. York, P.A. Kollman, AMBER 2020, in, University of California, San Francisco., 2020.
[63] Wang J, Wolf RM, Caldwell JW, Kollman PA, Case DA. Development and testing of a general amber force field. J Comput Chem 2004;25:1157–74.
[64] Jorgensen W, Chandrasekhar J, Madura J, Impey R, Klein M. Comparison of simple potential functions for simulating liquid water. J Chem Phys 1983;79:926–35.
[65] Maier JA, Martinez C, Kasavajhala K, Wickstrom L, Hauser KE, Simmerling C. ff14SB: improving the accuracy of protein side chain and backbone parameters from ff99SB. J Chem Theory Comput 2015;11:3696–713.
[66] Grest GS, Kremer K. Molecular dynamics simulation for polymers in the presence of a heat bath. Phys Rev A Gen Phys 1986;33:3628–31.
[67] Berendsen HJC, Postma JPM, van Gunsteren WF, DiNola A, Haak JR. Molecular dynamics with coupling to an external bath. J Chem Phys 1984;81:3684–90.
[68] Darden T, York D, Pedersen L. Particle mesh Ewald: an N·log(N) method for Ewald sums in large systems. J Chem Phys 1993;98:10089–92.
[69] Ryckaert J-P, Ciccotti G, Berendsen HJC. Numerical integration of the cartesian equations of motion of a system with constraints: molecular dynamics of n-alkanes. J Comput Phys 1977;23:327–41.
[70] Humphrey W, Dalke A, Schulten K. VMD: visual molecular dynamics. J Mol Graph Model 1996;14:33–8.
[71] L. Schrodinger, The PyMOL Molecular Graphics System, (2015).
[72] Pettersen EF, Goddard TD, Huang CC, Couch GS, Greenblatt DM, Meng EC, Ferrin TE. UCSF Chimera–a visualization system for exploratory research and analysis. J Comput Chem 2004;25:1605–12.
[73] D.A. Case, H.M. Aktulga, K. Belfon, I.Y. Ben-Shalom, J.T. Berryman, S.R. Brozell, D. S. Cerutti, I.T.E. Cheatham, G.A. Cisneros, V.W.D. Cruzeiro, T.A. Darden, N. Forouzesh, G. Giambaşu, T. Giese, M.K. Gilson, H. Gohlke, A.W. Goetz, J. Harris, S. Izadi, S.A. Izmailov, K. Kasavajhala, M.C. Kaymak, E. King, A. Kovalenko, T. Kurtzman, T.S. Lee, P. Li, C. Lin, J. Liu, T. Luchko, R. Luo, M. Machado, V. Man, M. Manathunga, K.M. Merz, Y. Miao, O. Mikhailovskii, G. Monard, H. Nguyen, K.A. O'Hearn, A. Onufriev, S.P.F. Pan, A.R.R. Qi, D.R. Roe, A. Roitberg, C. Sagui, S. Schott-Verdugo, A. Shajan, J. Shen, C.L. Simmerling, N.R. Skrynnikov, J. Smith, J. Swails, R.C. Walker, J. Wang, J. Wang, H. Wei, X. Wu, Y. Wu, Y. Xiong, Y. Xue, D. M. York, S. Zhao, Q. Zhu, P.A. Kollman, AMBER 2022, in, University of California, San Francisco., 2022.
[74] Bock A, Bermudez M, Krebs F, Matera C, Chirinda B, Sydow D, Dallanoce C, Holzgrabe U, De Amici M, Lohse MJ, Wolber G, Mohr K. Ligand binding ensembles determine graded agonist efficacies at a G protein-coupled receptor. J Biol Chem 2016;291:16375–89.
[75] Genheden S, Ryde U. The MM/PBSA and MM/GBSA methods to estimate ligand-binding affinities. Expert Opin Drug Discov 2015;10:449–61.
[76] Miller 3rd BR, McGee Jr TD, Swails JM, Homeyer N, Gohlke H, Roitberg AE. MMPBSA.py: an efficient program for end-state free energy calculations. J Chem Theory Comput 2012;8:3314–21.
[77] NCI-60 Cell Lines in the *In Vitro* Screen, ⟨https://dtp.cancer.gov/discovery_development/nci-60/cell_list.htm⟩, 11. 07. 2023.
[78] NCI-60 Screening Methodology, ⟨https://dtp.cancer.gov/discovery_development/nci-60/methodology.htm⟩, 11. 07. 2023.